SANDIA REPORT

SAND88–0112 • UC–70
Unlimited Release
Printed September 1988

Brine Inflow to WIPP Disposal Rooms: Data, Modeling, and Assessment

E. J. Nowak, D. F. McTigue, R. Beraun

Prepared by
Sandia National Laboratories
Albuquerque, New Mexico 87185 and Livermore, California 94550
for the United States Department of Energy
under Contract DE-AC04-76DP00789

Issued by Sandia National Laboratories, operated for the United States Department of Energy by Sandia Corporation.

Printed in the United States of America
Available from
National Technical Information Service
U.S. Department of Commerce
5285 Port Royal Road
Springfield, VA 22161

NTIS price codes
Printed copy: A05
Microfiche copy: A01

SAND88-0112
Unlimited Release
Printed September 1988

Distribution
Category UC-70

BRINE INFLOW TO WIPP DISPOSAL ROOMS: DATA, MODELING, AND ASSESSMENT

E. J. Nowak
Experimental Programs Division

D. F. McTigue
Fluid Mechanics and Heat Transfer Division I

R. Beraun
Experimental Programs Division
Sandia National Laboratories
Albuquerque, New Mexico 87185

ABSTRACT

A WIPP data base that characterizes brine movement and accumulation is summarized and analyzed. The data are interpreted in terms of a model for flow in a saturated porous medium. The model, summarized in this report, embodies the Darcy-flow assumption and storage due to linearly elastic compression of the salt and brine. Comparisons between model calculations and brine inflow rates measured in the WIPP show order-of-magnitude agreement for permeabilities in the range of 10^{-21} to 10^{-20} m^2 (1 - 10 nanodarcies). These values of permeability are in accord with independent, in situ determinations of permeability in the salt. Expected accumulations of brine in typical WIPP waste disposal rooms were calculated by numerical methods using a mathematical description for the brine inflow model. The expected brine accumulation in a disposal room was calculated to be in the range of 4 m^3 to 43 m^3 in 100 years. WIPP disposal rooms, filled with waste and backfilled, are expected to be virtually completely reconsolidated due to host rock creep in about 100 years, preventing further accumulation of brine. Calculations show that water-absorbing tailored backfill materials can readily absorb the maximum expected brine accumulations in WIPP disposal rooms while maintaining adequate mechanical strength.

TABLE OF CONTENTS

1. INTRODUCTION

1.1. Early and Related Studies

That the bedded salt being considered for radioactive waste disposal is not completely dry was recognized in the 1970's and early 1980's [1,2]. Analyses of water content in bedded rock salt generally [2,3,4] and in WIPP site-specific host rock salt [5,6,7] yielded estimates of approximately 0.1 wt% to 1 wt% unbound (not chemically bound) water. This unbound water can, under certain conditions, move to boreholes, sources of heat, access drifts, and storage rooms where it can accumulate and introduce humidity.

During the 1970's, concerns were expressed about the potentially deleterious effects of brine on the performance of waste repositories that contain radioactive waste [3,4]. At that time, Sandia National Laboratories formulated objectives and started a program to evaluate brine movement toward both heat-producing and contact-handled waste forms [8]. Laboratory studies of brine movement and inflow evolved from that program and were concentrated for several years primarily on the migration of brine toward heat-producing waste [1].

Several laboratory experiments and data analyses were done to quantify water release and identify parameters that control brine transport for small samples of bedded salt from southeastern New Mexico [1,3,9,10]. The results and mechanistic evaluations have been summarized [1]. No single operative mechanism for transport of brine to a heat source was found to explain the results.

A complex laboratory experiment was done in 1978-1979 to measure rates of water release to a heated borehole in a large block of bedded salt from southeastern New Mexico and to compare measured temperatures in the block with temperatures predicted by a mathematical model [11]. Measurable quantities of water were released. Data interpretations and analyses [1,11,12,13,14] yielded inconclusive evidence for any single mechanism of water transport [1].

In situ brine inflow experiments were conducted with both unheated and heated test boreholes in a southeast New Mexico potash mine [1,15]. Small water inflow rates to the unheated (before heaters were turned on) test boreholes were measured for periods of from two weeks (for two holes) to three months (for one hole). Heating increased the inflow rates, and inflow pulses were observed when the heater power was either increased or decreased. Quantities of salt encrustations in the boreholes measured during post-test investigations were consistent with the assumption that all the collected water had evaporated from inflowing brine and inconsistent with the vapor-phase model for brine inflow [1]. Observations about the salt encrustations were generally consistent with a stress-gradient model [1] and a fluid-inclusion-motion model [1].

Intermediate scale brine migration tests in isolated heated boreholes have been under way in the Asse mine in the Federal Republic of Germany [16,17]. These tests are located in a relatively pure, dry halite

anticline that resulted from diapirism. Water vapor from incoming brine was removed from the boreholes in gas streams, condensed, and measured. No water was collected in any of the boreholes before heating began. Relatively small quantities of water (approximately 0.1 kg per borehole in roughly 2 years) were collected during the heated phase [17]. These results are consistent with models for brine migration in relatively pure, dry halite. They are not necessarily applicable to bedded salt.

Several mechanistic models were initially proposed and developed for long term brine inflow toward nuclear waste disposal excavations in relatively pure salt deposits. The early models were focused on thermally stimulated transport by mechanisms such as: motion of brine inclusions in a temperature gradient caused by a temperature effect on solubility [18,19,20]; vapor phase transport through connected porosity driven by the water vapor pressure over heated brine [9,12]; and liquid transport through connected porosity driven by a stress gradient in the salt [1,13]. More recently, a model that couples more than one transport process was developed and used for a sensitivity study [21,22].

The mechanistic models were used to calculate predicted water accumulations under high-level waste repository conditions for a location in relatively pure bedded salt [1]. For that purpose, the brine inflow models were combined with thermomechanical models for temperature and stress distributions. Model parameters were derived from results of laboratory and in situ experiments [1]. Most of these experiments were done in or with rock salt from a single stratum found in a southeast New Mexico potash mine. Typical conditions for heat-producing high-level nuclear waste repositories in salt (2.16 kW per canister at emplacement, 150 kW/acre distributed thermal load) were chosen as a basis for the calculations [23]. Predicted accumulations of water were then calculated.

No more than 20 liters of water, either as brine or as vapor, were predicted to accumulate in a waste canister emplacement borehole in intact bedded salt during the first 1000 years after emplacement [1]. This prediction was based on the existing models for thermally-driven brine inflow and data primarily for a single stratum of bedded salt from southeastern New Mexico.

It was also recognized that brine seeps often associated with seams of other materials such as clays could deliver more water than the above estimate [1]. Therefore, this prediction was considered to be applicable to bedded salt generally as long as waste emplacement holes do not intersect seams of other materials such as clays and as long as brine content and brine behavior at elevated temperatures are not significantly different from those of the bedded salt samples that were tested [1]. Bedded salt is not pure on a macroscopic scale, and no quantitative criterion to identify seams of significant impurity was given.

Large-scale, site-specific, in situ experiments that duplicate as closely as possible the conditions in an actual repository were recommended to demonstrate the validity of the brine inflow predictions and to test the

existing mechanistic models [1]. In situ WIPP experiments were planned [24] for that purpose.

1.2. WIPP In Situ Experiments and Modeling

Sandia's WIPP-specific moisture release experiments, under way since April 1985, were designed to quantify brine inflow to four large (30 to 36 inch diameter) boreholes in the proposed WIPP disposal horizon [25,26,27,28,29]. The moisture release experiments were integrated with the near field effects/waste package full-scale interactions tests [24] that simulate near-reference repository conditions for defense high-level waste. Released water was measured both before and after heating began.

For several days prior to the initiation of heating, water was collected from each of the four test boreholes at rates in the range of 5 to 15 g/day [25,26,27,28,29]. This result highlighted the need for a site-specific isothermal model of brine movement toward and into WIPP excavations.

After heating began, the water collection rate for each of the four boreholes rose to a peak and then decreased [25,29]. A brine transport model that matches data for both isothermal and thermally stimulated brine inflows would derive support from both data sets.

The current data base for isothermal brine inflow to WIPP boreholes includes data from the WIPP Brine Sampling and Evaluation Program [30]. One of the purposes of this report is to evaluate these data and incorporate them into the data base for our modeling effort.

The need for a WIPP-specific brine transport model for both isothermal and non-isothermal conditions was recognized prior to 1987 [28], and a model was developed with data from the WIPP large scale in situ experiments [25,28,29]. This model is for transient Darcy flow in a porous medium. Elastic responses of the salt and brine cause the "storage" of brine that supports transient flow. Thermal effects are accounted for by including the thermal expansion of the brine and the host rock salt. The model is in good agreement with WIPP in situ brine inflow measurements when pre-excavation pore pressure (hydrostatic to lithostatic) and permeability (1 to 10 nanodarcy) are chosen in the ranges derived from independent WIPP in situ tests [31,32].

Isothermal brine flow to WIPP excavations was also calculated by Bredehoeft [33] using a similar Darcy flow model and data for WIPP host rock permeabilities. The calculated brine inflow rates were quite low, and calculated flows matched WIPP in situ inflow rates [25] for host rock permeabilities in the nanodarcy range.

A model for isothermal brine flow coupled with salt creep, and a parametric analysis, based on literature data for properties of salt, was reported for an idealized WIPP disposal room geometry [34,35]. This work is a credible beginning for exploring the consequences that such coupled

processes evoke. It attempts to account for both inelastic dilatation in the host rock and the evolving boundary conditions at the room walls. However, an important gap in current understanding is the lack of a realistic, quantitative model for the inelastic volumetric deformation (strain) during creep closure of excavations and the consequent permeability changes. This model will be discussed again later in this report. Nevertheless, it appears that both inelastic dilatation and evolving room conditions tend to weaken the brine inflow. Thus, our WIPP-specific model might be regarded as conservative, because it overpredicts brine inflow by neglecting these effects.

A prediction of brine inflow to WIPP TRU (transuranic) waste disposal rooms is needed to address the potential consequences of this brine for TRU waste isolation. It is desirable to assure that room contents remain in a solid rather than a fluid state. Brine inflow, room closure, and brine absorption by room backfill materials couple to determine whether the room contents remain solid.

The purpose of this report is to present a WIPP brine flow model, data, model calculations, and a quantitative assessment of the response of a backfilled, waste-containing disposal room to brine inflow. The brine inflow data imply a credible range of permeability values. Permeability values calculated from independent in situ measurements of fluid transport characteristics are given for comparison. A porous flow model, shown to match WIPP brine inflow data, is used to calculate brine inflow quantities to WIPP disposal rooms. Tailored room backfill materials are then shown to have adequate capacity to absorb the volume of brine that is expected to accumulate.

2. WIPP BRINE FLOW MODEL

A brine transport model for both isothermal and non-isothermal conditions in bedded salt was developed with data from the WIPP large scale in situ experiments [25,28,29]. This model is for transient Darcy flow in a porous medium. Elastic responses of the salt and brine account for the "storage" of brine that supports transient flow, and thermal effects are accounted for by including the thermal expansion of the brine and the host rock salt.

Any model for transient flow of fluid in a porous medium requires the stipulation of a mechanism of ''storage,'' that is, local changes of fluid mass per unit volume of the medium. In a rigid porous medium, the only available mechanism is compression, or the local density change, of the fluid. In a deformable porous medium, storage can be accommodated by dilatation of the solid skeleton and local compression of the solid, as well. Dilatation of the porous skeleton is the principal mechanism of interest in soil and rock mechanics, and is the cornerstone of ''consolidation'' theory. Rock salt, of course, exhibits plastic as well as elastic properties. It is, however, plausible that the immediate, elastic response of the salt and brine and the subsequent relaxation of the pore pressure by flow to the excavation are the predominant mechanisms of brine storage and transport, at least over short time scales.

For a linearly elastic skeleton, Biot [36] generalized the consolidation theory, and Rice and Cleary [37] later recast it in terms with straightforward physical interpretations. An extension of this model to account for non-isothermal effects, allowing for thermal expansion of the fluid and solid, has been presented recently [38,39].

The essence of the model is embodied in a diffusion equation for the pore pressure that, in certain special cases, reduces to:

$$\frac{\partial p}{\partial t} - c\nabla^2 p = b'\frac{\partial \theta}{\partial t}, \qquad (1)$$

where p is the fluid pore pressure, c is the fluid diffusivity, b′ is a source coefficient, and θ is the temperature. The fluid diffusivity, c, depends upon the permeability, fluid viscosity, and the elastic properties of the solid and fluid (see Appendix A). The source coefficient, b′, depends upon the thermal expansivities of the solid and fluid (see Appendix A). For isothermal conditions, the right hand side of (1) vanishes, and the classical diffusion equation for Darcy flow is recovered. Various special cases widely considered in hydrologic modeling are embedded in this formulation [25]. For non-isothermal problems in which conduction heat transfer dominates (i.e., small Peclet number), as is certainly true in salt, the source term in (1), which represents the generation of pore pressure by thermal expansion, must be evaluated from the simultaneous solution of the heat equation:

$$\frac{\partial \theta}{\partial t} - \kappa \nabla^2 \theta = 0 , \qquad (2)$$

where κ is the thermal diffusivity. Extended discussion of this system of equations as well as various solutions to representative initial value problems can be found in [38,39].

The explicit relationships between properties of salt and brine and the coefficients appearing in equations (1) and (2) are given in APPENDIX A of this report. The host rock salt permeability, k, and other properties of the host rock and brine appear in the fluid diffusivity, c.

In the data analyses that are discussed here, permeability values, k, were chosen to match or bracket the brine inflow data. Other values for the host rock and brine properties in the diffusivity, c, were taken from known properties of salt and saturated brines. The permeability values thus obtained were used to calculate brine inflow to WIPP disposal rooms with this model.

2.1. Isothermal Flow

Consider now an idealized model for the introduction of a mined drift into a deeply buried region. The rock is assumed to be homogeneous and isotropic, and the undisturbed stress state is taken to be lithostatic, i.e., isotropic, compressive, and equal in magnitude to the overburden load. The initial pore pressure in the neighborhood of the tunnel is assumed to be constant:

$$p(r,0) = p_0 . \qquad (3)$$

The pressure p_0 is expected to be between hydrostatic (about 6 MPa) and lithostatic (about 15 MPa) [25]; this has been corroborated by field measurements from which pore pressures of 8.3 MPa and 10.3 MPa were estimated [31]. Superimposed on the hydrostatic pressure is a portion of the increased mean stress induced by the presence of the tunnel. The fluid pressure then relaxes by Darcy flow toward the tunnel, and the load is transferred to the solid skeleton.

The pressure field corresponding to this sequence is governed by (1) with the right-hand side zero and with the initial condition (3) and boundary conditions:

$$p(a,t)=0 , \qquad (4)$$

$$\lim_{r \to \infty} p(r,t) = p_0 , \qquad (5)$$

where a is the excavation or borehole radius. Equation (4) simply states that the fluid is free to flow to the ''drained'' face, which is maintained at atmospheric pressure.

The solution to (1) and (3) to (5) is well known (e.g., [40]); the flux at the tunnel wall, $q(a,t_*)$, follows immediately from Darcy's law by differentiation:

$$q(a,t_*) = - \frac{kp_0}{\mu a} \frac{4}{\pi^2} \int_0^\infty \frac{\exp(-u^2 t_*)}{J_0^2(u) + Y_0^2(u)} \frac{du}{u} \tag{6}$$

where k is the permeability, μ is the fluid viscosity, $t_* = ct/a^2$ is the normalized time, and $J_0(x)$ and $Y_0(x)$ are zero-order Bessel functions of the first and second kind, respectively. Note that the sign of the flux is negative because it is in the (-r) direction. It is convenient also to introduce the asymptotic expansion for early time:

$$\lim_{t_* \to 0} q(a,t_*) = - \frac{kp_0}{\mu a} \left[\frac{1}{\sqrt{\pi}} t_*^{-1/2} + \frac{1}{2} - \frac{\sqrt{\pi}}{4} t_*^{1/2} + \frac{1}{8} t_* + \cdots \right] , \tag{7}$$

and that for late time:

$$\lim_{t_* \to \infty} q(a,t_*) = - \frac{kp_0}{\mu a} \left[\frac{2}{\ln(4t_*) - 2\gamma} - \frac{2}{[\ln(4t_*) - 2\gamma]^2} + \cdots \right] , \tag{8}$$

where $\gamma = 0.57722$ is Euler's constant. Values calculated with equations (6) - (8) are shown in Figure 1. Note that the flux falls off rapidly at early time, and changes only slowly for $t_* > 10$.

2.2. Flow to a Heated Borehole

Consider now the response of the salt and pore fluid to a constant heat flux delivered to a borehole wall. The appropriate initial and boundary conditions are then:

$$\theta(r,0) = \theta_0 , \tag{9}$$

$$\frac{\partial \theta}{\partial r}(a,t) = - \frac{q^h}{K} , \tag{10}$$

$$\lim_{r \to \infty} \theta(r,t) = \theta_0 \ , \tag{11}$$

where θ_0 is the ambient temperature, q^h is the heat flux at the borehole wall, K is the thermal conductivity, and

$$p(r,0) = p(a,t) = \lim_{r \to \infty} p(r,t) = 0 \ . \tag{12}$$

The initial and far-field conditions on the pressure, equation (12), neglect the non-zero ambient pressure considered in the foregoing section.

The solution to the temperature field (equations 2, 9-11) is well known [41]; substitution into the right-hand side of (1) yields a diffusion equation for the pressure with a known source term. This, in turn, can be solved by Laplace transform [38] to give the flux at the borehole wall:

$$q(a,t_*) = - \frac{kb'q^h}{\mu KR(1 - R^2)} \frac{2}{\pi} \int_0^\infty \frac{\exp(-\omega^2 t_*)[\Phi J_1(\omega) - \Psi Y_1(\omega)]}{[J_1^2(R\omega) + Y_1^2(R\omega)][J_0^2(\omega) + Y_0^2(\omega)]} \frac{d\omega}{\omega} \ , \tag{13}$$

where

$$\Phi = J_0(\omega)\Lambda_1 + Y_0(\omega)\Lambda_2 \ , \quad \Psi = J_0(\omega)\Lambda_2 - Y_0(\omega)\Lambda_1 \ ,$$

$$\Lambda_1 = J_0(R\omega)Y_1(R\omega) - Y_0(R\omega)J_1(R\omega) \ ,$$

$$\Lambda_2 = J_0(R\omega)J_1(R\omega) + Y_0(R\omega)Y_1(R\omega) \ ,$$

and $R^2 = c/\kappa$ is the ratio of the fluid and thermal diffusivities, or ratio of characteristic times for transport of heat and fluid mass, respectively. The early-time, asymptotic expansion of (13) is given by

$$\lim_{t_* \to 0} q(a,t_*) = - \frac{kb'q^h}{\mu KR(1 + R)} \left[1 - \frac{1}{\sqrt{2\pi}R} t_*^{1/2} + \frac{3 + R}{8R^2} t_* \cdots \right] . \tag{14}$$

2.3. Assumptions Inherent in the Model

It is our judgement that uncertainties associated with the assumptions in the model introduce uncertainty in brine inflow predictions for waste disposal rooms of no more than about an order-of-magnitude. Both the Darcy model itself and some of the assumptions invoked in order to represent the practical problems of interest are idealizations of very complex systems. It can be anticipated that some of these idealizations are conservative, in the sense that they tend to lead to overpredictions of brine flow at the WIPP, and some are "liberal," in the sense that they probably lead to underpredictions. The directions of uncertainties that may arise from some of the other model assumptions are difficult to assess at this time.

Assumptions that are likely to lead to overpredictions of brine inflow (conservative) include the following:

There exists a network of interconnected porosity extending outward without bound. This assumption implies a limitless reservoir of brine.

The far-field brine pressure is lithostatic. Aside from the stress perturbation due to the presence of the excavations, it is difficult to imagine a mechanism by which the pressure could rise above lithostatic.

Brine flow is radially symmetric (two dimensional). The effect of the third dimension is to weaken the flow by geometric spreading of the disturbance.

The backpressure from the room contents is negligible. Any backpressure due to interaction of the salt with solid, fluid, or gas in the storage room will mitigate the flow to the room.

Inelastic dilatation of the salt is neglected (see also below). Dilatation of the salt near the excavations due to inelastic mechanisms, such as opening grain boundaries, tends to decrease the pore pressures that drive flow.

Assumptions that are likely to lead to underpredictions of brine inflow ("liberal") include the following:

The storage of available brine in the host rock is due entirely to elastic compression of the brine and salt. Additional (inelastic) storage mechanisms would decrease the brine diffusivity and, therefore, increase the decay time for the flux. Thus, integrated fluxes over long time would be larger. The magnitude of the initial (maximum) flux, however, is unaffected by the storage.

Inelastic dilatation of the salt is neglected (see also above). Dilatation of the salt near the excavations due to inelastic mechanisms such as opening grain boundaries tends to increase the permeability in that region. However, calculations that account for extreme increases in permeability near the wall (given in Section 4.3.4 of this report) show relatively small increases in the cumulative brine flux, because the flow over long periods of time is controlled by the far-field properties.

The directions of uncertainties about possible effects of inelastic, volumetric deformations and of heterogeneities in the host rock salt are now difficult to assess. Such effects have not been the focus of the laboratory testing program for host rock salt. Also, the effects of heterogeneity are difficult to anticipate. Some further work to reduce these uncertainties will be described below. However, these effects on predicted brine inflow values are not expected to exceed an order of magnitude.

3. WIPP BRINE FLOW CHARACTERISTICS DATA BASE

Data pertinent to WIPP brine inflow predictions are available from several sources. Brine accumulations were measured by periodic bailing in boreholes located over a wide area of the WIPP facility. These measurements were part of the WIPP Brine Sampling and Evaluation Program [30]. Brine inflow rates were also calculated from moisture release data obtained from isothermal and heated boreholes in the Moisture Release Experiment for Rooms A1 and B in the WIPP [29]. Host rock permeability values are available from WIPP in situ brine and gas flow measurements that support the WIPP Plugging and Sealing Program [31]. The data from these sources are described in the following sections.

3.1. WIPP Brine Sampling Data

Deal and Case [30] monitored 54 drillholes throughout the WIPP, most of them for about 500 days. They show graphical results for the time histories of the total flux for 20 holes. The flow rates to two of the holes, BX02 and DH37, fell essentially to zero after 600 days. The flow rates to the remaining 18 holes at the end of the reporting period are considered here (Table 1). Hole A1X02 exhibited a nearly monotonic decay in flow rate for nearly 400 days, but then experienced a steady increase in flow rate. The value entered in Table 1 for A1X02 hole corresponds to the value at the end of the period of declining rate. The recorded flow rates represent the integrated flux over the borehole surface areas, and are recorded in Table 1 in units of liters per day, i.e., a volume flow rate.

3.2. WIPP Moisture Release Data

Full-scale simulations of high-level waste repository environments [24] have been under way at the WIPP site since April, 1985 in two large (5.5 x 5.5 x 90 m) rooms, designated A1 and B. The rooms are at the WIPP waste disposal horizon in the bedded salt of the Salado Formation. In each of these rooms is an array of vertical boreholes, heated by electric resistance heaters. The boreholes are 0.38 m in radius, and the heated length is 3.10 m; the Room B hole designated B041 is an exception, with radius 0.46 m and heated length 3.45 m. The heaters in Room A1 are designed to simulate defense high-level waste at near-reference conditions of 18 W/m^2 thermal loading; each heater is operated nominally at 470 W. Room B simulates overtest conditions, at 1500 W per heater. Two of the heated holes in each room are instrumented to monitor temperatures and moisture release. Moisture from the borehole walls is removed continuously in the vapor phase by nitrogen circulated through the holes. The nitrogen is passed through cold traps and desiccant canisters, and the mass of water collected is recorded. Details of the experimental setup and procedures are given in [25,26].

Prior to the start of heating, the initial moisture release rate for each of the four test boreholes fell within the range of 5 to 15 g/day. Upon heating, the 470 W holes in Room A1 yielded peaks of 15 to 17 g/day

within about 10 days, and the flow rates declined subsequently to about 10 g/day after 100 days. Flow to the 1500 W holes in Room B continued to increase over a longer period, rising to peak rates of 80 to 90 g/day after 100 days, and slowly decreasing throughout the remainder of the test. Cumulative quantities of water were 4.3 kg at 441 days from Room A1 boreholes and 36 to 38 kg at 600 days from Room B boreholes. These moisture release data will be compared with calculations from the model to establish a credible permeability range that represents brine transport in the host rock.

3.3. WIPP Host Rock Permeabilities from Independent In Situ Flow Measurements

Permeability values in the range of 10^{-21} to 10^{-20} m^2 (1 to 10 nanodarcy) or lower have been derived for intact WIPP host rock from independent *in situ* measurements of brine flow during fluid transport experiments [31,42,43]. Independent measurements of the both gas and brine permeability of the salt at the WIPP facility horizon have been made using constant-pressure and pressure-decay methods in 6.5 cm radius boreholes [31,32,42]. These tests showed that permeabilities *near the drift wall* were mostly of the order of 10^{-20} to 10^{-18} m^2 (10 to 1000 nanodarcy) or higher in some cases. *A few meters into the wall*, permeabilities were of the order of 10^{-22} to 10^{-20} m^2 (0.1 to 10.0 nanodarcy). Measurements in the WIPP waste-handling shaft at levels above the proposed disposal horizon confirm the range of 10^{-21} to 10^{-20} m^2 (1 to 10 nanodarcy) for undisturbed host rock salt [43]. The permeability range implied by comparisons between model calculations and brine inflow measurements will be compared with these results.

3.4. Data Reduction

3.4.1. Radial Darcy Flow Model for Isothermal Data Reduction

An idealized model was introduced previously [25] to investigate the order-of-magnitude agreement of observed fluxes with the proposed Darcy flow mechanism. This model was described above. In particular, it was assumed that mined faces and boreholes introduce zero-pressure surfaces into a region of porous salt in which the brine is initially at hydrostatic pressure. (It is easy to argue that the initial pressure may be as large as lithostatic, but this changes the initial conditions only by a factor of about two. The uncertainty in the permeability is expected to be much greater.) In this case, the Darcy flux, q, to a circular borehole scales in the following fashion [25]:

$$q \propto \frac{kp_0}{\mu a}, \qquad (15)$$

where k is the permeability, p_0 is the initial pressure, μ is the brine viscosity, and a is the borehole radius. This factor is multiplied by a

time-dependent function of order unity that represents the decay of the flux as the pressure disturbance propagates away from the hole. The characteristic time over which this decay takes place, t_o, is given by:

$$t_o = \frac{a^2}{c} , \tag{16}$$

where c is the fluid diffusivity. For elastic rock, the fluid diffusivity scales like:

$$c \simeq \frac{kK}{\mu} , \tag{17}$$

where K is an elastic modulus for the porous skeleton. It can be argued from the model that, for WIPP salt, the appropriate modulus and viscosity yield a diffusivity of the order of

$$c \simeq 1.1 \times 10^{14} k \quad m^2/s , \tag{18}$$

where the permeability is given in units of m^2.

Previous calculations [29,39] suggest that the brine diffusivity is of the order of 10^{-7} m^2/s. For a borehole of radius 0.05 m, then equation (16) gives a characteristic time of the order of 2.5×10^4 s, or about seven hours. Therefore, after 500 days, the drillholes in the WIPP can be expected to be in the asymptotic limit of ''late'' time. In this case, the flux can be approximated by the first term in the series given by equation (8):

$$|q| = \frac{kp_o}{\mu a} \frac{2}{\ln(4ct/a^2) - 2\gamma} , \tag{19}$$

where $\gamma \simeq 0.57722$ is Euler's constant.

3.4.2. Permeabilities from Brine Sampling Data

Deal and Case [30] report the dimensions of the holes from which they collected and measured brine, so that it is simple to calculate the vertical wall area of each. These values are recorded in Table 2. The average Darcy flux (or "Darcy velocity") for each hole is easily calculated by dividing the integrated volume flux by the total borehole area. This step is not taken here, because the comparison can be misleading. If the flow does occur by a Darcy mechanism, then the Darcy velocity is expected to scale inversely with the borehole radius. Thus, the appropriate measure for a hole-to-hole comparison in this context is the product of the Darcy

flux and the borehole radius. The values of this product appear in the fifth column of Table 2, labeled "qa".

The values for the product of the Darcy flux times borehole radius, which are proportional to the total flow rates per unit length of borehole, center around 3 x 10^{-12} m^2/s. The maximum value is for hole NG252, at 2.1 x 10^{-10} m^2/s. This hole samples an anomaly in the WIPP host rock; consequences of this anomaly will be discussed below.

The apparent permeability was calculated for each borehole using values for "qa", the Darcy flux times the borehole radius, and equation (19). In particular, it was assumed that the initial pressure is p_o = 6.0 x 10^6 Pa, corresponding approximately to hydrostatic pressure for a depth of 600 m. The brine viscosity is taken to be 1.6 x 10^{-3} Pa·s. The time was assumed to be t = 4.32 x 10^7 s (500 days) for every hole. The diffusivity was assumed to be given by (18). Finally, for each drillhole, values for the flux times the radius, qa, are known (Table 2).

Thus, the only unknown parameter is the apparent permeability, k_{app}. The explicit relationships between the properties of salt and brine and the coefficients appearing in the above relationships are given in APPENDIX A of this report. Also given in that appendix are the typical properties for WIPP salt that were used.

The nonlinear relationship for "k_{app}", represented by equations (18) and (19) is then easily solved numerically. The results of this exercise are shown in the last column of Table 2. The values shown may be read directly as nanodarcies (10^{-21} m^2 ≈ 1 nd).

Figure 2 shows a histogram of the logarithm of the apparent permeabilities given in Table 1. The mean of the log is -20.45 (k = 3.5 x 10^{-21} m^2, or about 3.5 nanodarcy), and the standard deviation of the logarithm of k_{app} is 0.81. Also shown is the lognormal distribution corresponding to these values. These limited data and the highly idealized model suggest a lognormal distribution for the apparent permeability. This is a common observation in other rocks.

The highest value of apparent permeability shown in Figure 2, 4.4 x 10^{-19} m^2, is likely to be anomalously high. That datum represents the brine inflow rate to borehole NG252, a borehole that is known to intersect a horizontal fracture associated with Marker Bed 139 [30]. Thus, the ideal smooth borehole model from which the apparent permeability was calculated can be expected to yield an anomalous value that does not correctly characterize the host rock salt. A fracture can introduce a large surface area for inflow; if this flow is then averaged over the borehole wall area only, the calculated flux and the apparent permeability will be erroneously large. A model that accounts explicitly for flow to both the borehole and a large intercepted fracture should yield a more nearly representative value for the apparent permeability. For example, an order-of-magnitude estimate of the additional inflow from a 12 m radius crack with a very small aperture yields an apparent permeability of 10^{-20} m^2, a value that is in better agreement with the other permeability values.

3.4.3. Permeabilities from Isothermal Moisture Release Data

Before the heaters were turned on in the instrumented boreholes in Rooms A1 and B, moisture was collected in all four holes for a few days [26]. The integrated mass flow rates were in the range of 5 to 15 g/day, which, averaged over the borehole area, corresponds to a Darcy flux of 0.85 to 2.6 x 10^{-11} m/s. The product of the flux times the borehole radius, a = 0.38 m, is then in the range: qa = 3.2 to 9.9 x 10^{-12} m^2/s. In comparing these values to those calculated from the IT measurements (Table 2), it should be noted that the latter represent flows at much later time ($t >> t_o$).

The apparent permeabilities for the moisture-release holes were calculated in a fashion similar to the approach used above, and the resulting values were in the range of 10^{-21} m^2 to 10^{-20} m^2. In this case, however, the flow rates measured in the pre-heating stage do not reflect very late time, and the asymptotic solution, equation (19), is not accurate. Using the full integral solution (6), the same initial condition, p_o = 6.0 x 10^6 Pa, and t = 2.1 x 10^7 s (8 months), the observed range of fluxes requires permeabilities in the range k ≃ 2.4 to 9.3 x 10^{-21} m^2. These values are quite consistent with those required to represent the IT data (Figure 2), and, again, are consistent with independently measured *in situ* permeabilities [31,42,43].

It should be noted that these permeability values are our best estimate so far and represent a significant improvement over an interim study [25]. In that study, it was assumed that the test boreholes for the WIPP moisture release experiments simply intercepted brine flow to the test rooms (WIPP Rooms A1 and B). From the scaling relation for the Darcy flux to a circular hole or tunnel (equation 15), the permeability is expected to scale like $k \simeq q\mu a/p_o$, where "a" is the appropriate length scale. The length scale for the test rooms is 3.5 m; for the test boreholes it is 0.4 m. Therefore, the apparent permeabilities reported in the interim study are about an order of magnitude larger than the apparent permeabilities calculated here. Here, the length scale used is the test borehole radius of 0.38 m. This scale is appropriate for the model, because the pressure field in the neighborhood of the test room should change relatively slowly, and flow to the boreholes should respond primarily to the local pressure field around the borehole. Time scales for excavations are given in terms of radius and diffusivity in equation 16.

3.4.4. Permeabilities and Modeling from Results of Thermally-Driven Brine Transport Tests

Two cases of thermally-driven transport of brine in salt have been analyzed in view of a Darcy-flow model. The data considered were from both laboratory and field experiments. In these tests, the flux of brine to a heated borehole was monitored over time. The model [38,39] assumes that the salt is a fluid-saturated, porous, thermoelastic material. Upon heating,

pressure is induced in the brine due to the thermoelastic compression of the matrix and the thermal expansion of the brine relative to that of the solid. The brine flows toward the borehole, which is maintained at atmospheric pressure.

It is important to emphasize that the transport processes in this model are identical to those considered in the isothermal problems in other sections of this report. The capacitance of the salt is due to elastic compression of the brine, the mineral grains, and the bulk rock. The resistance to flow is represented by the classical Darcy law. Only the driving force is different from that treated in the isothermal configurations. Here, the brine is pressurized by thermal expansion; in the isothermal problems the brine is under an initial pressure due to the ambient state of stress in the salt.

Model results for brine flow due to thermal effects serve several important functions in the present context. First, comparisons to laboratory and field measurements provide independent tests for the validity of the Darcy flow model. If model calculations prove to be consistent with observations for thermally-driven flows, then one has greater confidence in applying the model to isothermal flows, in which the driving forces are different, but the fundamental transport processes are the same. Second, these data afford an opportunity to check for internal consistency in the material properties invoked. For example, one would hope to find that properties such as permeability, indicated by comparisons of model calculations and measurements, are similar for both thermally-driven and isothermal flows. Finally, the thermally-driven flow experiments provide the only detailed, well-controlled, transient data available at this time. This is of critical importance, because the brine influx issue for the WIPP involves transient flows, which, in the present modeling context, require knowledge of two material properties: capacitance and permeability or diffusivity and permeability. Fits of model calculations to data for transient flows yield both parameters. This again provides a check for consistency; one is able to compare to independent estimates of the material properties.

3.4.4.1. WIPP Heated Borehole Experiment

A detailed, transient analysis of coupled equations (1) and (2) for the heated boreholes at the WIPP has not been attempted as yet. Over the time scale of the field experiment, two- and possibly three-dimensional effects are inevitable, particularly because the test holes are of finite length and are part of a large array of heated holes. In addition, measured borehole wall temperatures in Room B ranged from ambient (about 28°C) to nearly 130°C. Over this range, the brine viscosity, μ, is expected to decrease about one order of magnitude, and the thermal expansion coefficient of the brine is expected to increase by at least a factor of two. Thus, the linearized theory discussed above is somewhat limited in the present application.

Nonetheless, it is worthwhile to perform some idealized calculations based on the linear model in order to determine if it captures essential features of the data. Figure 3 shows data for the cumulative flux of water to borehole B042 at the WIPP; recall that the measurements represent the volume of pure water collected. The flow rate rose steadily to a peak value of approximately 0.08 l/day at about 100 days, and declined slowly thereafter [25]. Also shown in Figure 3 are calculations based on equation (13) and the material properties shown in APPENDIX A. The viscosity (μ = 0.60 x 10^{-3} Pa•s) and fluid thermal expansion coefficient (α_f = 5.6 x 10^{-4} K^{-1}) used for these calculations are estimated values for a temperature of 95°C, which corresponds to the borehole wall temperature at the time of the peak flux (100 days).

As in the isothermal case, the observations are bracketed by the calculated flow for k = 10^{-21} to 10^{-20} m^2 (See Figure 3.). For k = 10^{-21} m^2, the fluid diffusivity is c = 2.8 x 10^{-7} m^2/s and R = 0.33; for k = 10^{-20} m^2, the fluid diffusivity is c = 2.8 x 10^{-6} m^2/s and R = 1.1.

There is a qualitative discrepancy between the measured and calculated response at early time, which may be due to omissions in the simplified model. In particular, note from (14) that the model fluid flux starts at a finite value at zero time, and decays monotonically thereafter. This is due, at least in part, to the assumed instantaneous application of a constant heat flux to the borehole (10). Analysis that accounts for a wall heat flux with a finite rise time indicates that the fluid flux to the borehole rises from zero, peaks, and subsequently decays, as observed in the experiment. This alone would change the computed cumulative curves shown in Figure 3 from concave-up to concave-down at early time. The assumed (constant) low viscosity, appropriate for later time, also contributes to the overestimation of the flux at early time.

A further check on the scaling relations revealed by the linearized model is possible by noting from (14) that the magnitude of the flux predicted is simply

$$q_o = \frac{kb'q^h}{\mu KR(1 + R)} \quad . \tag{20}$$

The remaining terms in (13) and (14) are functions of time of order unity. Table 3 shows estimates of the peak flux measured in each borehole; in the low-power boreholes (A1041, A1042), this peak was reached on a scale of roughly 10 days; in the high-power boreholes (B041, B042), the peak was reached after approximately 100 days. Equation (20) is then evaluated for each hole using the properties given in Appendix A, with the viscosity and fluid expansion coefficient adjusted to values appropriate to the borehole wall temperature at the time of the peak fluid flux.

The scale for the flux (20) emerging from the model analysis is again of the correct order of magnitude for permeabilities in the range 10^{-21} to 10^{-20} m^2.

3.4.4.2. Salt Block II Experiment

The Salt Block II experiment [11] was performed some ten years ago in support of the WIPP project. In this experiment, a right circular cylinder of salt, 1 m long and 1 m in diameter, was obtained from a potash mine near Carlsbad. A 13 cm diameter borehole was located on the axis of the cylinder. An electric resistance heater was placed in the borehole, and the heater power was stepped up over a range of 0.2 to 1.5 kW, with each power level held for a period of several days. The fluid driven to the borehole was collected in a low-pressure dry gas stream and absorbed externally in a desiccant. Temperatures interior to the block were monitored by an array of thermocouples.

A one-dimensional idealization of the Salt Block II configuration has been modeled [44] using the "porothermoelasticity" theory described in Section 2. of this report. The block is assumed to be at a constant initial temperature, and the initial excess pore pressure is taken to be zero. The heat flux at the borehole is represented by a linear ramp up to a constant value for each stage of the experiment. The heat flux at the outer boundary is represented by a heat transfer coefficient. The pore pressure at the borehole is taken to be zero, and the outer jacket is assumed to be impermeable, so that the pressure gradient vanishes there. The radial normal stress is zero at both the inner and outer radii.

The coupled heat transfer, fluid flow, and solid deformation problem reduces, in this configuration, to a pair of diffusion equations for the temperature and fluid pressure. The equations are nonlinear, because the model allows for temperature-dependent properties, including the thermal conductivity and brine viscosity. The problem is solved numerically by the method of lines.

The numerical solver is coupled to a parameter-estimation code that seeks the set of specified parameters that results in the best fit to the experimental data. In this case, for example, the thermocouple data are fitted by the solution to the conduction calculation to determine the thermal conductivity and the heat transfer coefficient at the outer boundary. These values are then used in the coupled problem for the fluid flow, with the fluid diffusivity and a source coefficient considered unknown. Here, the calculated fluid flux at the borehole is compared to the experimental measurements.

The inverse calculations were carried out for the first three stages of the Salt Block II experiment, at 0.2, 0.4, and 0.6 kW. An excellent representation of the temperature data was obtained, and the inferred properties are consistent with independent determinations. For example, for constant thermal properties, the procedure indicates a conductivity of 5.2 W/m/K, which is typical of measurements for WIPP salt [45]. The result

of central interest here is that for the brine diffusivity (the permeability divided by a capacitance and the brine viscosity). The simulations were performed for a fixed value of permeability, $k = 10^{-21}$ m^2 (1 nanodarcy), and they allowed for a temperature-dependent viscosity.

The best fit to the fluid flux data was obtained for a reference (18°C) diffusivity value of $c = 0.70 \times 10^{-7}$ m^2/s. At 28°C, this corresponds to a diffusivity of $c = 0.87 \times 10^{-7}$ m^2/s. For a permeability of 10^{-21} m^2 (1 nanodarcy) and a viscosity of 1.6×10^{-3} Pa•s, this implies a capacitance of $7.2\ 10^{-12}$ Pa^{-1}. A previous estimate of the capacitance, based on independent estimates of the elastic properties of the brine and salt [29] was 5.7×10^{-12} Pa^{-1}, and the corresponding diffusivity for $k = 10^{-21}$ (1 nanodarcy) was $c = 1.1 \times 10^{-7}$ m^2/s.

Thus, a fit of model calculations to data from the Salt Block II experiment yields a fluid diffusivity only about 25% lower than that computed from independent estimates of the elastic properties. This agreement may be regarded as quite good, given the uncertainty in several of the material properties. It might be noted, as well, that one would expect the apparent diffusivity derived from a one-dimensional model simulation to be less than the apparent diffusivity for the multidimensional configuration. The effect of the finite length of the cylinder is to allow axial losses of heat and pressure and to allow some relaxation of the pore pressure by axial expansion of the solid matrix. Thus, the one-dimensional, radial model tends to overpredict the fluid flux, which must be accommodated in the parameter estimation scheme by reducing the apparent transport coefficients.

3.4.4.3. Inferences from Analyses of Thermally-Driven Brine Transport Tests

Both laboratory and field experiments that measured brine flow rates stimulated by heating of salt from a borehole have been analyzed using a Darcy flow model. Although the driving force for the flows is different from those that operate under isothermal conditions, the mechanisms of "storage" (or capacitance) and flow resistance are identical. Thus, study of these configurations has a direct bearing on the isothermal problems that are of more immediate concern at the WIPP. In particular, these experiments offer opportunities to perform independent model validation studies, and to infer material properties by matching model calculations and data.

Calculations with the Darcy flow model for WIPP brine fit data from the Salt Block II experiment with very good agreement. The Salt Block II experiment is currently the only transient flow test that has been analyzed completely in light of the Darcy flow model. Comparisons between the model calculations and experimental data for the first three stages of the test (0.2, 0.4, 0.6 kW) are excellent. An inverse calculation yields a wholly empirical fluid diffusivity measurement, based principally on the decay rate of the borehole flux. This, when combined with an assumed permeability, provides a direct measure of the capacitance of the salt.

The result is only about 25% higher than the capacitance calculated based on the elasticity model and independent estimates of the properties.

The heated borehole experiments at the WIPP also appear to be well represented by the linear, thermoelasticity model, and the observed cumulative flux is bracketed by calculations for permeabilities of 10^{-21} m^2 and 10^{-20} m^2 (1 and 10 nanodarcies), values that are in good agreement with independently-made in situ measurements [31,42,43].

4. PREDICTIONS OF BRINE INFLOW TO WIPP DISPOSAL ROOMS

4.1. Choice of Permeability Values and Other Model Parameters

The range of 1 to 10 nanodarcies (10^{-21} to 10^{-20} m^2) was chosen as the experimentally-supported expected permeability range for calculating expected brine inflow to WIPP TRU waste disposal rooms and for idealized scoping calculations. The experimental support for that range is shown as a histogram in Figure 4. The data cluster very strongly in this range. In situ measurements of brine permeabilities in relatively undisturbed WIPP host rock salt and in other rock types such as anhydrite all fall within the chosen range [31,42,43].

Explicit relationships between the properties of salt and brine and coefficients appearing in brine flow model relationships are given in APPENDIX A of this report. Also given there are the material properties for WIPP salt that were used in the model.

4.2. Scoping Calculations for Idealized Geometries

The calculations in this section serve to illustrate that the prediction of WIPP brine inflow cannot be divorced entirely from physical models. For example, measurements made in boreholes of roughly the same size reveal nothing about the scaling of brine inflow to larger excavations. Furthermore, one does not know from tests done on a small time scale how to extrapolate brine inflow to much longer times. A model is necessary to translate the brine flow pattern surrounding a test borehole and its evolution in time to the brine flow pattern and time history of flow surrounding a disposal room.

These calculations also serve to illustrate the magnitudes of brine inflow that one might expect from a Darcy flow mechanism and the sensitivity of inflow to model variations such as flow geometry and consideration of the transient flow component.

4.2.1. Boundary and Initial Conditions and Material Properties

It is assumed that the mined room introduces surfaces at atmospheric pressure into a region initially at some uniform pressure value. One might expect that the initial pressure is bounded between hydrostatic (for the depth beneath the water table) and lithostatic (for the repository depth). The variation of hydrostatic or lithostatic pressure with depth is negligible within a few tens of meters of the repository. More detailed discussion of the initial condition, including the effect of the altered mean stress field due to the presence of a cavity, is given in [25]. For simplicity, the initial pressure in the following Sections (4.2.2 - 4.2.5) is taken to be hydrostatic:

$$p_0 = 6.0 \times 10^6 \text{ Pa}; \qquad (21)$$

the choice of lithostatic initial pressure would simply increase the calculated fluxes and volumes by a factor of about two. The cumulative flux is evaluated at 200 years:

$$t = 6.31 \times 10^9 \text{ s.} \tag{22}$$

It has been estimated previously, based on independent measurements of the mechanical properties of salt [e.g., 45], that the diffusivity for WIPP salt is

$$c \simeq (1.1 \times 10^{14})k \quad m^2/s \ , \tag{23}$$

where k is given in units of m^2.

Permeability (k) values in the range of 10^{-21} to 10^{-20} m^2 (1 to 10 nanodarcy) or lower have been derived for intact WIPP host rock from independent *in situ* measurements of brine flow during fluid transport experiments [31,42,43]. It should be stressed that these estimates are subject to improvement from more detailed modeling and field measurements. However, they are consistent with the current WIPP data base.

$$k \simeq 10^{-21} \text{ to } 10^{-20} \text{ m}^2 \tag{24}$$

The brine viscosity at 28°C is

$$\mu = 1.6 \times 10^{-3} \text{ Pa}\cdot\text{s} \ . \tag{25}$$

Equations (24) and (25) were used to calculate the diffusivity, c, using equation (23).

4.2.2. Radial Flow to an Isolated Tunnel

The geometry for a radial flow to an isolated tunnel is shown in Figure 5. This model accounts for flow from above and below the tunnel. It neglects, of course, the effects of the rectangular shape of the room, but those effects damp out for later time. The results for this model geometry have been discussed in a previous report [25].

The flux to the tunnel, q, is given by:

$$|q(a,t)| = \frac{kp_0}{\mu a} \frac{4}{\pi^2} \int_0^\infty \frac{\exp\left(-u^2 ct/a^2\right)}{J_0^2(u) + Y_0^2(u)} \frac{du}{u} \ , \tag{26}$$

where a is the radius, and J_0 and Y_0 are zero-order Bessel functions of the first and second kind, respectively. The total volume of brine is determined by multiplying the flux by the area of the tunnel walls (vertical side walls, floor, and ceiling for an equivalent rectangular room). A calculation for an equivalent waste disposal room follows.

The circumference of a reference waste disposal room (33 ft by 13 ft) is 28 m (92 ft); thus, the effective radius of an equivalent circular tunnel is

$$a = 4.5 \text{ m} \tag{27}$$

and the appropriate area is the sum of the side-wall, floor, and ceiling areas:

$$A_2 = 2548 \text{ m}^2 \text{ .} \tag{28}$$

Equation (26) then gives the following total brine inflow volumes at the end of 200 years ,

$$V \text{ (for } k = 10^{-21} \text{ m}^2) = 6.7 \text{ m}^3 \tag{29}$$

$$V \text{ (for } k = 10^{-20} \text{ m}^2) = 40.6 \text{ m}^3 \tag{30}$$

4.2.3. Steady State Flow to a Line Sink

At sufficiently long time, the pressure field does not relax to zero everywhere as implied by the diffusion model, but approaches a steady-state condition in which the far-field is hydrostatic and there is recharge at the water table. See Figure 6 for this geometry. This model should yield a smaller brine inflow value, because the higher transient flow at early times is not included. In this case, for $a/d \ll 1$, the flux at the room walls, q_{wall}, is given by [25]:

$$|q_{wall}| = \frac{kp_0}{\mu a} \frac{-1}{\ln(a/2d)} \text{ ,} \tag{31}$$

and the cumulative flux is obtained simply by multiplying $|q_{wall}|$ by the wall area and total time of interest.

The WIPP facility horizon is about 600 m below the water table, i.e.,

$$d = 600 \text{ m .} \tag{32}$$

Equation (31), along with equations (27), (28), and (32), then gives the following total brine inflow values at the end of 200 years:

$$V \text{ (for } k = 10^{-21} \text{ m}^2) = 2.6 \text{ m}^3 \text{ ,} \tag{33}$$

$$V \text{ (for } k = 10^{-20} \text{ m}^2) = 26.3 \text{ m}^3 \text{ .} \tag{34}$$

4.2.4. Horizontal Flow (1-D) to an Isolated Room

This case represents a situation in which there is no vertical flow, perhaps because of impermeable, horizontal clay or anhydrite seams above and below the disposal room. (See Figure 7.) The flow is allowed to spread outward without bound, because adjacent rooms in a panel of rooms are not considered.

This problem is exactly analogous to the cooling of a plane half-space, and the pressure profile takes the well-known form:

$$p = p_0 \, \mathrm{erf} \, \frac{x}{2\sqrt{ct}} \quad , \tag{35}$$

where p_0 is the initial pressure, x is the distance away from the wall, and c is the diffusivity. The flux at the wall, q (e.g., in units of $m^3/s/m^2$), is determined from equation (35) using Darcy's law:

$$|q(0,t)| = \frac{kp_0}{\mu\sqrt{\pi ct}} \quad , \tag{36}$$

where k is the permeability, and μ is the brine viscosity. The cumulative flux, Q (e.g., in units of m^3/m^2), is obtained from (36) by integration:

$$Q(t) = \frac{2kp_0}{\mu\sqrt{\pi c}} \, t^{1/2} \quad . \tag{37}$$

The cumulative volume of brine is determined by multiplying (37) by the area of the vertical side walls of the room.

The vertical side-wall area for the model room is

$$A_1 = 728 \ m^3 \quad . \tag{38}$$

Thus, for 1-D flow from an unbounded domain, equation (37) predicts a cumulative volume,

$$V \ (\text{for } k = 10^{-21} \ m^3) = 0.73 \ m^3 \quad , \tag{39}$$

$$V \ (\text{for } k = 10^{-20} \ m^3) = 2.33 \ m^3 \quad . \tag{40}$$

4.2.5. Horizontal Flow (1-D) to a Room in a Panel

The next case to be considered is for one-dimensional flow to one room among an array of similar rooms separated by pillars of finite width. See Figure 8. In this case, the pressure disturbance can spread only to the centerline of the pillar, where it must be symmetric because of flow to the

next room. This problem simply looks like the cooling of a finite slab, and the solution is again well known:

$$p = p_0 4 \sum_{n=0}^{\infty} \frac{\sin \lambda_n x}{\lambda_n L} \exp\left(-c\lambda_n^2 t\right) \quad , \tag{41}$$

where L is the thickness of the pillar between rooms and $\lambda_n L = (2n + 1)\pi$. The flux at the wall, q, is again obtained from Darcy's law by differentiation of (41):

$$|q(0,t)| = \frac{kp_0}{\mu L} 4 \sum_{n=0}^{\infty} \exp\left(-c\lambda_n^2 t\right) \quad . \tag{42}$$

The cumulative flux is obtained by integration of (42):

$$Q(t) = \frac{kp_0 L}{\mu c} 4 \sum_{n=0}^{\infty} \frac{1 - \exp\left(-c\lambda_n^2 t\right)}{(\lambda_n L)^2} \quad , \tag{43}$$

and the total volume is again obtained by multiplying by the vertical area of the side walls.

For 1-D flow from a finite domain between rooms, using A_1 from above, equation (38), and

$$L = 30.5 \text{ m} \ ,$$

equation (43) gives:

$$V \text{ (for } k = 10^{-21} \text{ m}^2) = 0.37 \text{ m}^3$$

$$V \text{ (for } k = 10^{-20} \text{ m}^2) = 0.37 \text{ m}^3$$

These values are identical, because the drainage process is essentially complete after 200 years even at the lower diffusivity. This is apparent from evaluation of the characteristic time, $(L/2)^2/c$, which takes the value 2.1×10^9 s (67 years) for $k = 10^{-21}$ m^2 and 2.1×10^8 s (6.7 years) for $k = 10^{-20}$ m^2. Also note that the cumulative flux is significantly less than for the isolated room (unbounded flow region), because there is simply a smaller pressurized region upon which to draw.

4.2.6. Comparison of Results for Idealized Geometries

Results from the highly idealized models considered here are collected in Table 4 for ease of comparison. Some observations can be made from these calculated results:

Cumulative brine inflow to waste disposal rooms does not scale linearly with host rock permeability. An order-of-magnitude increase in permeability results in significantly less than an order-of-magnitude increase in accumulated brine. This non-linearity occurs, because the characteristic time for the transient component of brine inflow is a function of the permeability.

The choice of a flow model has a significant influence on the calculated quantity of accumulated brine in waste disposal rooms.

If vertical brine flow is strongly inhibited by bedding planes, brine inflow will be much smaller than for the isotropic flow case, and adjacent rooms in a panel will also cause significantly reduced flow to a disposal room. Bedding planes of unusually high permeability could increase brine inflow.

The transient contribution to brine inflow is significant during the first 200 years for a waste disposal room.

The expected brine inflow volume to a waste disposal room is to be no more than a few tens of m^3 in 200 years, based on this model

4.3. Calculations of Expected Brine Accumulation in WIPP Disposal Rooms

The WIPP brine flow model was used to calculate, by numerical methods, expected brine accumulation values for the WIPP reference disposal room geometry (4 m (13 ft) high by 10 m (33 ft) wide by 91 m (300 ft) long). These calculations yield more accurate estimates of brine inflow than were obtained from the above scoping calculations for idealized geometries.

Transient, two-dimensional numerical analyses were performed for three different disposal room configurations: (1) a room with reference

dimensions placed between adjacent rooms in a reference panel configuration (30.5 m (100 ft) wide salt pillars between rooms); (2) a reference room sufficiently distant from other rooms so that there are no brine flow interactions with any other excavations; (3) a room that is larger than reference in order to simulate, with void space, a high-permeability disturbed zone surrounding a reference room

Values for model parameters were chosen to represent expected or reasonable ranges. The permeability range of 1 to 10 nanodarcies was chosen, as described above, as a the expected range for the calculation of brine infow. Equation (18) was used to calculate the diffusivity. Two values for the initial far field (undisturbed) pore pressure were chosen: hydrostatic pressure (6 MPa) and lithostatic pressure (15 MPa). These pressure values are reasonable bounds for the expected undisturbed pore pressure.

Brine accumulations were obtained by integrating inflow rates from the moment of excavation (t = 0). Actual accumulations in WIPP disposal rooms are expected to be smaller, because water from inflowing brine will be removed by evaporation into ventilation air during early times when the inflow rate is highest.

Brine inflow into waste-containing, backfilled WIPP disposal rooms is expected to cease within 100 years due to consolidation of room contents by creep closure [46] and the resulting increase in pore pressure within the rooms. The present calculations were carried out to 200 years for completeness and ease of comparison with the scoping calculations presented in the previous section of this report.

The numerical model constructed for these studies was based on several simplifications:

The variation of hydrostatic or lithostatic pressure with depth was assumed to be negligible within a few tens of meters of the repository.

The effect of closure on room geometry was neglected. Closure increases the brine flow path and could decrease brine inflow.

Pressure build-up during creep closure due to the compression of room contents is not accounted for. Increasing room pressure would decrease the driving force for brine influx. Therefore, neglecting this interaction is conservative.

Symmetry of brine flow was invoked to simplify the numerical model.

Because of the large geometrical dimensions associated with the model, the specification of impermeable boundaries for all exterior element boundaries vertically above the repository is a good approximation of the real situation.

Details of the physics, algorithm, model geometry, material properties, and boundary and initial conditions are presented elsewhere [47,48]. The mesh is a two-dimensional Cartesian finite element mesh that was generated by the PATRAN-G [49] finite element graphics package. Upon completion of the mesh, it was translated to the equivalent finite difference network. The diffusion equation for pore pressure, equation (1), was solved numerically using Q/TRAN [50].

4.3.1. WIPP Disposal Room in a Panel

Brine inflow to a typical waste disposal room in a panel was calculated for hydrostatic and lithostatic initial (undisturbed host rock) pore pressures and permeability values of 1 and 10 nanodarcies.

The expected range of brine accumulation in a TRU disposal room is 4 m^3 in 100 years for hydrostatic initial pore pressure and 1 nanodarcy permeability, to 43 m^3 in 100 years for lithostatic initial pore pressure and 10 nanodarcy permeability. Calculated cumulative volumes are plotted in Figures 9 through 12 for times to 200 years.

4.3.2. Sensitivity to Initial Pore Pressure

Because of the linearity of the model, the brine flux and cumulative brine inflow are proportional to the initial pore pressure. This is shown by the analytical results discussed previously (equations 6,36,42), and corroborated by the numerical calculations. At a permeability of 1 nanodarcy, the cumulative brine volume in 100 years increases from 4 m^3 to 9 m^3 when the initial pore pressure is increased from hydrostatic to lithostatic (from 6 to 15 MPa). At 10 nanodarcy, the cumulative volume increases from 17 m^3 to 43 m^3 for the same change in the initial pore pressure. Figures 13 and 14 illustrate the sensitivity to the initial pore pressure.

4.3.3. Sensitivity of Brine Inflow Host Rock Permeability

Increasing the host rock permeability from 1 to 10 nanodarcy increases the brine inflow by a factor that lies between 4 and 5. There is a nonlinear relationship between cumulative brine volume and permeability, because the rate at which the transient brine inflow decays depends upon the permeability. The change in brine inflow rate is significant at these permeability values during the first 100 years. These results are illustrated in Figures 15 and 16.

4.3.4. Effect of a High-Permeability Disturbed Zone Surrounding a Waste Disposal Room

The development of a high-permeability disturbed zone surrounding a waste disposal room is unlikely to cause a significant increase in brine

inflow. The worst-case disturbed zone surrounding a room has infinite permeability. Such a disturbed zone can be simulated by moving the atmospheric-pressure boundary into the host rock and calculating room inflow at that boundary. Host rock salt within that boundary is assumed to be hydraulically isolated from the far field; thus the brine that it contains experiences no driving force (pore pressure gradient) for flow. A disturbed zone 10 m thick above and below a room and 5 m thick on either side was simulated by increasing the height of the room by 20 m and the width of the room by 10 m. Calculated results are plotted in Figures 17 and 18 for permeabilities of 1 and 10 nanodarcy. The initial pore pressure was taken to be lithostatic pressure (15 MPa). In this simulation, the disturbed zone increased the calculated 100-year cumulative brine inflow volume from 43 to 52 m^3 for the maximum expected permeability of 10 nanodarcies. For 1 nanodarcy, the increase was from 9 m^3 to 17 m^3.

4.3.5. Effect of Adjacent Rooms in a Panel

The effect of adjacent rooms in a panel on brine inflow is to decrease the 100-year cumulative brine volume by approximately 25% when the host rock permeability is 10 nanodarcy (10^{-20} m^2). This comparison is shown in Figure 19 for hydrostatic pressure as the initial pore pressure and in Figure 20 for lithostatic pressure. The comparison is between the calculated brine inflow to a room far from other rooms and the previously-presented calculated inflow to a room in a panel of rooms.

5. ASSESSMENT OF BRINE INFLOW EFFECTS ON WIPP DISPOSAL ROOMS

An assessment of brine inflow effects on disposal rooms is necessary to address the potential consequences of this brine for TRU waste isolation. It is desirable to assure that room contents remain in a solid (non-flowing) rather than a fluid state. The final state of room contents will depend on the relative rates of brine inflow and consolidation of room contents by creep closure. Consolidation is expected to be virtually complete within 100 years [46].

It was determined that water-absorbing tailored backfill materials can readily absorb the maximum credible expected 100-year brine accumulations in WIPP disposal rooms without becoming brine-saturated. This assessment was done by coupling expected maximum credible brine accumulations in disposal rooms, the expected maximum reconsolidation time of 100 years [46], and estimated absorption capacities for room backfill materials. The data and calculations that were used are described below.

5.1. Expected Brine Accumulations in WIPP Disposal Rooms

Expected accumulations of brine in typical WIPP waste disposal rooms were calculated by numerical methods using a mathematical description for the brine inflow model. These numerical calculations were given in Section 4.3 of this report. WIPP disposal rooms filled with waste and backfilled are expected to become virtually completely compacted due to host rock salt creep in about 100 years [46], preventing further accumulations of brine. Therefore, brine accumulations during the first 100 years were used here. For a comparative reference, a typical room has an initial excavated volume of approximately 3600 cubic meters (950,000 gallons). A summary of 100-year brine accumulations from the numerical calculations is as follows:

Host Rock Permeability, Nanodarcies	Pre-Excavation Pore Pressure	Cumulative Brine Volume in Typical Waste Disposal Room after 100 Years, Cubic Meters, (Gallons), (% of Initial Room Volume)
1	Hydrostatic	4 m^3 (1000 gal) (0.11%)
1	Lithostatic	9 m^3 (2400 gal) (0.25%)
10	Hydrostatic	17 m^3 (4500 gal) (0.47%)
10	Lithostatic	43 m^3 (11000 gal) (1.19%)

Other scoping calculations (in Section 4.2 of this report) for idealized room geometries (long cylinders) provided confirmation of the above results, yielding volumes in the range of approximately 1 to 40 m^3.

The worst credible case 43 m^3 of brine is 1.2% of the initial room volume, about the same as the quantity of brine in the salt that was removed by mining the room. To gain some visual perspective on the relative magnitude, one can visualize a layer of brine 4.6 cm (1.8 inches)

deep on the floor of a 4 m (13 foot) high room as the equivalent of 43 m^3 of brine in a typical empty WIPP waste disposal room. It will be shown in the next section that backfill materials such as crushed salt and bentonite clay can readily absorb such a quantity of brine without becoming saturated or degraded.

5.2. Absorption of Accumulated Brine by Backfills

As-mined (granular) WIPP salt backfill alone can absorb 40 m^3 of accumulated brine in a disposal room (93% of the predicted worst case 43 m^3), according to conservative estimates of room backfill quantity and water absorption capacity. The absorption capacity is the difference between the measured water content (0.5 wt% or less) of mined WIPP salt backfill material and the water content (2.5 wt%) of mechanically strong blocks pressed from WIPP crushed salt. Details of brine absorption capacity calculations for crushed salt are given in the next section of this report.

A tailored backfill material mixture of 30 wt% bentonite in crushed WIPP salt can absorb 120 m^3 of accumulated brine. That is about 3 times the predicted worst case 43 m^3 in 100 years. This result was also based on conservative estimates of room backfill quantity and water absorption capacity for bentonite. Bentonite in this WIPP room backfill mixture has the capacity to absorb 90 m^3 of water (chemically bound) without becoming water-saturated [51]. This absorption capacity takes into account water that would be pre-absorbed from WIPP air at approximately 70% relative humidity [52], an actual humidity value that is currently being measured by Sandia in WIPP boreholes (ongoing Room D brine inflow and humidity experiments). Details of brine absorption capacity calculations for bentonite/crushed salt mixtures are given in the next section of this report.

Tailored backfill mixtures with bentonite as a water absorber have always been considered in WIPP backfill investigations. Bentonite mixed with 70 wt% WIPP crushed salt is currently being tested in WIPP simulated CH TRU waste technology experiments [53]. The long-term stability of bentonite in contact with WIPP brines is supported by reported Sandia studies [54].

5.3. Capacities of Room Backfill Materials for the Absorption of Brine

Absorption capacity values were calculated in the following way. A minimum backfill volume in each disposal room was calculated for a maximum reasonable packing density of waste drums. An empty space two feet thick at the top of each room allows for backfill emplacement with commercially available solids handling and conveying equipment. The water absorption capacities of crushed WIPP salt and a mixture of 30 wt% bentonite in crushed WIPP salt, both as emplaced backfill materials, were calculated from published data. Then the quantity of accumulated brine that the

backfill in a room can absorb was calculated by combining backfill quantities and absorption capacities with the measured water content of WIPP brine.

WASTE DISPOSAL ROOM VOLUME AVAILABLE FOR BACKFILL

Basis:

33 ft wide by 13 ft high by 300 ft long waste disposal rooms

2 ft diameter by 3 ft tall drums

3 layers of drums (drums stacked 3-high)

150 rows of drums, maximum, in each layer

15 drums, maximum, in each row

2 ft empty gap between emplaced backfill and room back (roof)

Calculations:

volume of each drum = $\pi(1)^2(3)$ = 9.4248 ft^3

maximum number of drums per room = 15(150)3 = 6750 drums per room

maximum volume occupied by drums = 6750(9.4248) = 63,617 ft^3

volume of empty gap above backfill = 2(33)300 = 19,800 ft^3

volume of disposal room after excavation = 13(33)300 = 128,700 ft^3

minimum volume available for backfill = 128,700 - 63,617 - 19,800
= 45,283 ft^3

per cent of initial room volume available for backfill =
45,283 ÷ 128,700 x 100 = 35%

WATER ABSORPTION CAPACITY OF WIPP CRUSHED SALT

Basis:

as-emplaced water content [55,56] = 0.5 wt%

maximum water content in strong crushed salt blocks [57] = 2.5 wt%

net allowed water content gain = 2.5 - 0.5 = 2.0 wt%

bulk density of crushed salt backfill material [55] = 1300 kg/m^3

Calculations:

minimum water absorption capacity = (0.02)1300
= 26 kg water/m^3 crushed salt

volume of disposal room after excavation = 128,700(0.3048)^3
= 3644 m^3

volume available for backfill = 3644(0.35) = 1276 m^3
= 35% of room volume

quantity of water that can be absorbed in the crushed salt backfill in a room = 26(1276) = 33,164 kg water absorbed/room

WATER ABSORPTION CAPACITY OF A MIXTURE OF 30 WT% BENTONITE WITH CRUSHED WIPP SALT

Basis:

water content of bentonite equilibrated with water vapor in disposal room air [52] = 0.15 g/g bentonite

total water capacity of emplaced bentonite [52] = 0.3 g/g bentonite

available water gain in bentonite backfill [52] = 0.15 g/g bentonite

bulk density of 30 wt% bentonite in WIPP crushed salt [55] = 1300 kg/m^3

Calculations:

water absorption capacity of bentonite in mixture = 0.15(0.3)1300 = 58.5 kg water/m^3 backfill mixture

water absorption capacity of crushed WIPP salt in mixture = 0.02(0.7)1300 = 18.2 kg water/m^3 backfill mixture

total water absorption capacity of backfill mixture = 58.5 + 18.2 = 76.7 kg water/m^3 backfill mixture

volume of disposal room after excavation = 128,700(0.3048)^3
= 3644 m^3

volume available for backfill = 3644(0.35) = 1276 m^3
= 35% of room volume

quantity of water that can be absorbed in the crushed salt/bentonite backfill mixture in a room = 76.7(1276) = 97,869 kg water absorbed/room

ABSORPTION OF WIPP BRINE BY DISPOSAL ROOM BACKFILLS

Basis:

maximum expected 100-year brine accumulation = 43 m^3 brine/room

density of WIPP brines [58] = 1.2 g/cm^3 = 1200 kg/m^3

water in WIPP brine "weeps" [58] = 0.6877 kg water/kg brine

quantity of water that can be absorbed by a room backfill of 100% crushed WIPP salt (see above) = 33,164 kg water/room

quantity of water that can be absorbed by a room backfill mixture of 70 wt% crushed salt/30 wt% bentonite (see above) = 97,869 kg water/room

Calculation for 100% crushed WIPP salt:

quantity of brine that can be absorbed by crushed WIPP salt backfill = 33,164 ÷ ((0.6877)(1200)) = 40 m^3 brine/room

per cent of 100-year brine accumulation that can be absorbed by WIPP crushed salt room backfill = 40 ÷ 43 = 93%

Calculation for 70 wt% WIPP crushed salt/30 wt% bentonite mixture:

quantity of brine that can be absorbed by mixture = 97,869 ÷ ((0.6877)(1200)) = 119 m^3 brine/room

per cent of 100-year brine accumulation that can be absorbed by crushed salt/bentonite room backfill mixture = 119 ÷ 43 = 277%

6. SUMMARY AND CONCLUSIONS

Water-absorbing tailored backfill materials can readily absorb the maximum expected brine accumulations in WIPP disposal rooms while maintaining mechanical strength and without becoming brine-saturated. Crushed WIPP salt alone can absorb almost all of the maximum expected brine accumulation. Salt creep is expected to virtually completely reconsolidate backfilled waste disposal rooms within 100 years, increasing the pore pressure in the room and stopping brine accumulation at that time. The expected 100-year brine accumulations were calculated with a predictive Darcy flow model for the movement of brine to WIPP excavations. The model, data base, expected brine volumes, brine absorption capacity of backfills, and needs for further work are summarized below.

6.1. Brine Inflow Model

We have a predictive model for the movement of brine to WIPP excavations from WIPP rock salt. This model is based on well-known physical processes of groundwater flow in granular deposits. All values for model parameters are consistent with independent measurements of brine and host rock salt properties, and brine movements calculated from the model are consistent with the body of existing data for brine accumulations in WIPP underground test boreholes. The details of the model and its applicability to WIPP rooms and test boreholes rest upon a number of assumptions that are being subjected to further testing. Experiments are underway in the WIPP specifically for that purpose [59].

According to the model, brine flows in intergranular spaces within the polycrystalline host rock salt under the driving force of preexisting hydrostatic (groundwater head of approximately 900 psi, or about 6 MPa) or lithostatic (overburden pressure of approximately 2200 psi, or about 15 MPa) pore pressure toward the atmospheric pressure at excavation walls.

The capability of the host rock salt to allow flow under this driving force, commonly expressed as a "permeability", is very small, in the range of 1 to 10 nanodarcies. These permeability values are in good agreement with independent WIPP in situ fluid flow measurements. The Darcy flow process in geologic materials is well understood, and the describing mathematical formalism is accepted by the scientific community.

6.2. Brine Inflow Data Base

The range of permeability values for the model, 1 to 10 nanodarcy, was derived from WIPP in situ tests and brine sampling data, and data from moisture release experiments. Permeability values in this range or lower have been derived for intact WIPP host rock from several independent in situ measurements of brine flow in the host rock salt and in interbeds such as anhydrite (e.g., Marker Bed 139). These in situ measurements constitute the most reliable source for the host rock permeability. The measurements were made at the disposal horizon and at intervals above in the waste-

handling shaft. Permeabilities in the disturbed zone near drift walls were greater than 10 nanodarcy.

Darcy flow permeability values calculated from IT Corporation's WIPP brine sampling data were described reasonably well by a typical lognormal distribution with a logarithmic mean of 3.5 nanodarcy. A lognormal distribution of permeability values is a common observation for other rock types. Permeability values similarly calculated from Sandia moisture release data (Rooms A1 and B) are in the range of 2 to 9 nanodarcy.

It is our judgement that the uncertainty in permeability is in the order-of-magnitude range. The details of the model and its applicability to WIPP rooms and test boreholes also rest upon a number of assumptions. For the most part, these assumptions are likely to yield conservatively large values for long term brine inflow. Critical assumptions concerning flow mechanisms are being tested with ongoing and planned WIPP experiments. Potential inaccuracies stemming from idealized geometries are being investigated with more detailed numerical calculations.

6.3. Calculated Brine Accumulations

The maximum expected brine accumulation in a disposal room was calculated to be 43 m^3. Expected accumulations of brine in typical WIPP waste disposal rooms during 100 years after waste emplacement were calculated by numerical methods using a mathematical description for the brine inflow model. WIPP disposal rooms, filled with waste and backfilled, are expected to be virtually completely reconsolidated due to host rock creep in about 100 years, preventing further accumulation of brine. Expected cumulative brine volumes were in the range of 4 m^3 to 43 m^3. Other, less complex calculations for idealized room geometries (long cylinders) provided confirmation of these values, yielding volumes in the range of about 1 to 40 m^3. The maximum expected accumulation, 43 m^3, is 1.2% of the initial room volume, about the same as the quantity of brine in the salt that was removed by mining the room.

6.4. Absorption of Accumulated Brine by Room Backfills

Mined WIPP salt backfill alone can absorb 40 m^3 of accumulated brine in a disposal room (93% of the expected worst case of 43 m^3), according to conservative estimates of room backfill quantity and water absorption capacity. The absorption capacity is the difference between the measured water content (0.5 wt% or less) of mined WIPP salt backfill material and the water content (2.5 wt%) of physically strong blocks pressed from WIPP crushed salt.

A tailored backfill material mixture of 30 wt% bentonite in crushed WIPP salt can absorb 120 m^3 of accumulated brine, about 3 times the worst credible case of 43 m^3. The bentonite in this WIPP room backfill mixture has the capacity to absorb 90 m^3 of water without becoming water-saturated. This absorption capacity takes into account water that would be pre-

absorbed from WIPP air at approximately 70% relative humidity, an actual humidity value that is currently being measured by Sandia in WIPP boreholes (ongoing Room D brine inflow and humidity experiments).

Tailored backfill mixtures with bentonite as a water absorber have always been considered in WIPP backfill investigations. Bentonite mixed with 70 wt% WIPP crushed salt is currently being tested in WIPP simulated CH TRU waste technology experiments. The long-term stability of bentonite in contact with WIPP brines is supported by reported Sandia studies.

6.5. Needs for Further Work

Remaining uncertainties in the host rock permeability, in other brine inflow model parameters, and in mechanistic details of the model should be addressed. Experimental work and model development are needed.

The following in situ measurements are recommended to reduce uncertainties and test aspects of the existing model:

- host rock permeabilities to brine throughout the WIPP underground and in all representative strata
- host rock pore pressures beyond and within the disturbed zone
- brine inflow rates to excavations of significantly different scale, including large room-shaped excavations
- brine inflow rates to identifiably different strata
- responses of host rock flow properties and pore pressures to changes in stress and strain

Scale-up predictions and certain mechanistic assumptions in the model concerning pore pressure and flow paths will be tested with ongoing and planned WIPP in situ tests in small (4-inch) and large (36-inch) diameter boreholes [59].

Laboratory measurements of shear strain and permeability may aid the development of relationships between host rock creep and flow properties.

Brine inflow model development is also recommended. Permeability variations that depend on stratum, general location, host rock stress, and host rock creep (disturbed zone development) should be considered in the model. The host rock salt is heterogeneous, and, to be complete, the model should be developed further to reflect that heterogeneity. Experimental testing of model assumptions can be guided by sensitivity studies.

7. REFERENCES

1. H. C. Shefelbein, Brine Migration: A Summary Report, SAND82-0152, Sandia National Laboratories, September 1982.

2. R. I. Bradshaw and W. C. McClain, eds., Project Salt Vault: A Demonstration of the Disposal of High-Activity Solidified Wastes in Underground Salt Mines, ORNL-4555, Oak Ridge National Laboratory, April 1971.

3. J. J. Hohlfelder, Measurement of Water Lost from Heated Geologic Salt, SAND79-0462, Sandia National Laboratories, July 1979.

4. J. J. Hohlfelder, Volatile Content of Rock Salt, SAND79-2349, Sandia National Laboratories, April 1981.

5. D. W. Powers et al, eds., Geologic Characterization Report, Waste Isolation Pilot Plant (WIPP) Site, Southeastern New Mexico, SAND78-1596, Sandia National Laboratories, December 1978.

6. E. Roedder and H. E. Belkin, "Application of Studies of Fluid Inclusions in Permian Salado Salt, New Mexico, to Problems of Siting the Waste Isolation Pilot Plant," in Scientific Basis for Nuclear Waste Management, Vol. 1, G. J. McCarthy, ed., Plenum Press, New York, 1979, pp. 313-321.

7. S. R. Black, et al, eds., Results of Site Validation Experiments, Vol. II, Supporting Document 10, "Brine Content of Facility Interval Strata," U. S. Department of Energy, Waste Isolation Pilot Plant, March 1983.

8. S. J. Lambert and H. C. Shefelbein, A Strategy for Investigation of Fluid Migration in Evaporites (Waste Isolation Pilot Plant-WIPP), SAND79-1889, Sandia National Laboratories, March 1980.

9. G. R. Hadley and G. W. Faris, Revised Theory of Water Transport in Rock Salt, SAND80-2398, Sandia National Laboratories, October 1981.

10. J. J. Hohlfelder and G. R. Hadley, Laboratory Studies of Water Transport in Rock Salt, SAND79-1519, Sandia National Laboratories, November 1979.

11. J. J. Hohlfelder, Salt Block II: Description and Results, SAND79-2226, Sandia National Laboratories, June 1980.

12. G. R. Hadley, Salt Block II: Brine Migration Modeling, SAND81-0438, Sandia National Laboratories, October 1981.

13. T. G. Trucano, Computer Modeling of Stress States Associated with Fluid Migration Experiments, SAND81-2008, September 1981.

14. O. George Jr., Computer Thermal Modeling for the Salt Block II Experiment, SAND79-2250, Sandia National Laboratories, October 1980.

15. R. I. Ewing, Preliminary Moisture Release Experiment in a Potash Mine in Southeastern New Mexico, SAND81-1318, Sandia National Laboratories, November 1981.

16. T. Rothfuchs, D. Lubker, A. Coyle, and H. Kalia, Nuclear Waste Repository Simulation Experiments, Asse Salt Mine, Federal Republic of Germany: Annual Report 1983, prepared for Office of Nuclear Waste Isolation, Battelle Memorial Institute, Columbus OH, October 1984.

17. A. J. Coyle, J. Eckert, and H. Kalia, Brine Migration Test Report: Asse Salt Mine, Federal Republic of Germany, BMI/ONWI-624, prepared for Office of Nuclear Waste Isolation, Battelle Memorial Institute, Columbus OH, January 1987.

18. D. R. Olander et al, Thermal Gradient Migration of Brine Inclusions in Salt, ONWI-208, Office of Nuclear Waste Isolation, October 1980.

19. G. H. Jenks, Effects of Temperature, Temperature Gradients, Stress, and Irradiation on Migration of Brine Inclusions in a Salt Repository, ORNL-5526, Oak Ridge National Laboratory, July 1979.

20. P. F. Gnirk et al, State-of-the-Art Review of Brine Migration Studies in Salt, SAND81-7054, for Sandia National Laboratories, by RE/Spec Inc., September 1981.

21. J. L. Ratigan, "A Finite Element Formulation for Brine Transport in Rock Salt," Proc. Int. J. Numerical Anal. Methods Geomechanics, 8, No. 3, 1984, p. 225.

22. J. L. Ratigan, "A Sensitivity Study of Brine Transport into a Borehole Containing a Commercial High-Level Waste Canister," Nuclear Technology, 67, No. 2, 1984.

23. H. C. Claiborne et al, Expected Environments in High-Level Nuclear Waste and Spent Fuel Repositories in Salt, ORNL/TM-7201, Oak Ridge National Laboratory, August 1980.

24. M. A. Molecke, "WIPP Waste Package Testing on Simulated DHLW: Emplacement," in: Scientific Basis for Nuclear Waste Management VIII, C. M. Jantzen, et al., eds., Materials Research Society Symposia Proceedings, Vol. 44, Materials Research Society, Pittsburgh, 1985, pp. 265-271.

25. E. J. Nowak and D. F. McTigue, Interim Results of Brine Transport Studies in the Waste Isolation Pilot Plant (WIPP), SAND87-0880, Sandia National Laboratories, May 1987.

26. E. J. Nowak, Preliminary Results of Brine Migration Studies in the Waste Isolation Pilot Plant (WIPP), SAND86-0720, Sandia National Laboratories, May 1986.

27. E. J. Nowak, "Brine Migration Studies in the Waste Isolation Pilot Plant (WIPP)," in: Waste Management '86 - Waste Isolation in the U. S. Technical Programs and Public Education, Vol. 2, Proceedings of the Symposium on Waste Management at Tucson, Arizona, March 2-6, 1986, pp. 153-158.

28. E. J. Nowak, "Brine Movement in Waste Isolation Pilot Plant (WIPP) Tests," SAND86-1094A, Sandia National Laboratories, presented in the symposium on: Origin & Evaluation of Brines in the Subsurface, American Chemical Society National Meeting, Anaheim, CA, September 7-12, 1986.

29. D. F. McTigue and E. J. Nowak, "Brine Transport in the Bedded Salt of the Waste Isolation Pilot Plant (WIPP): Field Measurements and a Darcy Flow Model," in: Scientific Basis for Nuclear Waste Management X, Materials Research Society Symposia Proceedings, Vol. 84, Materials Research Society, Pittsburgh, 1988, accepted for publication.

30. D. E. Deal and J. B. Case, IT Corporation, Brine Sampling and Evaluation Program, Phase I Report, DOE-WIPP-87-008, prepared by the Engineering and Technology Department of the Management and Operating Contractor, Waste Isolation Pilot Plant Project for the U. S. Department of Energy, June 1987.

31. E. W. Peterson, P. L. Lagus and K. Lie, WIPP Horizon Free Field Fluid Transport Characteristics, SAND87-7164, prepared by S-CUBED, A Division of Maxwell Laboratories, Inc., for Sandia National Laboratories, December 1987.

32. J. C. Stormont, E. W. Peterson and P. L. Lagus, Summary of and Observations about WIPP Facility Horizon Flow Measurements through 1986, SAND87-0176, Sandia National Laboratories, May 1987.

33. J. D. Bredehoeft, "Will Salt Repositories Be Dry?," EOS, Transactions, American Geophysical Union, 69, No. 9, March 1, 1988, p. 121.

34. S. Niou and J. M. Pietz, "Coupled Brine Migration and Stress Analysis for Repository Room Saturation in Bedded Salt," in proceedings, 28th US Symposium on Rock Mechanics, Tucson AZ, June 29 - July 1, 1987, pp. 601-608.

35. S. Niou, J. Tyburski, J. Pietz and J. Case, "Coupled Fluid Flow and Creep Analysis for Room Saturation of a Salt Repository: Parametric Analysis," presented at: 1987 International Waste Management Conference, Session 7, American Society of Mechanical Engineers, December 2, 1987.

36. M. A. Biot, "General Theory of Three Dimensional Consolidation," Journal of Applied Physics, 12, (1941), 155-164.

37. J. R. Rice and M. P. Cleary, "Some Basic Stress-Diffusion Solutions for Fluid-Saturated Elastic Porous Media with Compressible Constituents," Reviews of Geophysics and Space Physics, 14, (1976), 227-241.

38. D. F. McTigue, A Linear Theory for Porous Thermoelastic Materials, SAND85-1149, Sandia National Laboratories, September 1985.

39. D. F. McTigue, "Thermoelastic Response of Fluid-Saturated Porous Rock," J. Geophysical Research, 91, 1986, pp. 9533-9542.

40. J. Crank, The Mathematics of Diffusion, Clarendon Press, Oxford, 1979, p. 87.

41. H. S. Carslaw and J. C. Jaeger, Conduction of Heat in Solids, Oxford University Press, Oxford, 1959, p. 338.

42. G. J. Saulnier and J. D. Avis, Interpretation of Hydraulic Tests Conducted in the Waste-Handling Shaft at the Waste Isolation Pilot Plant (WIPP) Site, SAND88-7001, prepared for Sandia National Laboratories, report in preparation.

43. J. C. Stormont, Division 6332, Sandia National Laboratories, personal communication about in situ brine flow and permeability measurements, reports in preparation.

44. D. F. McTigue, "Flow to a Heated Borehole in Fluid-Saturated Thermoelastic Rock (abstract)," EOS Transactions of the American Geophysical Union, 68, (1987) p. 1295.

45. R. D. Krieg, Reference Stratigraphy and Rock Properties for the Waste Isolation Pilot Plant (WIPP) Project, SAND83-1908, Sandia National Laboratories, 1984.

46. H. S. Morgan, "Estimate of Time Needed for TRU Storage Rooms to Close," Memorandum to D. E. Munson, Sandia National Laboratories, Division 1521, June 2, 1987.

47. R. Beraun, "Brine Flow Numerical Modeling for the WIPP Disposal Rooms," Memorandum to Distribution, Division 6332, Sandia National Laboratories, January 22, 1988.

48. R. Beraun, "Fluid Flow-Heat Transfer Equivalence," Memorandum to Distribution, Division 6332, Sandia National Laboratories, February 29, 1988.

49. PDA Engineering, Inc., PATRAN-G User's Guide, Volumes I and II, Santa Ana, CA, 1980.

50. F. A. Rockenbach, Q/TRAN, PDA Engineering, Inc., Santa Ana, California, May 1986.

51. R. Pusch, "Highly Compacted Bentonite - A Self-Healing Substance for Nuclear Waste Isolation," in: Scientific Basis for Nuclear Waste Management, Vol. 3, J. G. Moore, ed., Plenum Press, New York, 1981.

52. B. M. Butcher, "Bentonite Water Sorption," Memorandum of Record, Sandia National Laboratories, January 6, 1988.

53. M. A. Molecke, Test Plan: WIPP Simulated CH and RH TRU Waste Tests: Technology Experiments (TRU TE), Sandia National Laboratories, April 1986.

54. J. Krumhansl, Observations Regarding the Stability of Bentonite-Based Backfills in a High-Level Waste Repository in Rock Salt, SAND83-1293, Sandia National Laboratories, June 1984.

55. T. W. Pfeifle, Backfill Material Specifications and Requirements for the WIPP Simulated DHLW and TRU Waste Technology Experiments, SAND85-7209, Sandia National Laboratories, July 1987.

56. D. J. Holcomb and M. Shields, Hydrostatic Creep Consolidation of Crushed Salt with Added Water, SAND87-1990, Sandia National Laboratories, October 1987.

57. J. C. Stormont and C. L. Howard, Development, Implementation and Early Results: Test Series C of the Small-Scale Seal Performance Tests, SAND87-2203, Sandia National Laboratories, December 1987.

58. C. L. Stein and J. L. Krumhansl, Chemistry of Brines in Salt from the Waste Isolation Pilot Plant (WIPP), Southeastern New Mexico: A Preliminary Investigation, SAND85-0897, Sandia National Laboratories, March 1986.

59. E. J. Nowak, Test Plan: Brine Inflow and Humidity Experiments in Room D, Sandia National Laboratories, January 1988.

7. TABLES

Hole number	Flow Rate l/day	Area m^2	Radius m
IG202	0.014	5.20	0.0572
IG201	0.025	5.91	0.0572
NG252	0.250	0.26	0.0190
A1X01	0.026	4.84	0.0508
A1X02	0.010	5.74	0.0508
A2X01	0.025	4.87	0.0508
A2X02	0.015	5.13	0.0508
A3X01	0.023	4.91	0.0508
A3X02	0.001	4.93	0.0508
BX01	0.055	4.87	0.0508
DH36	0.250	4.38	0.0444
DH38	0.055	4.04	0.0444
DH40	0.005	4.34	0.0444
DH42	0.030	4.35	0.0444
DH42A	0.095	3.44	0.0444
DH35	0.002	4.42	0.0444
L1X00	0.028	3.72	0.0380
DH215	0.004	1.22	0.0508

Table 1. Observed flow rates for WIPP boreholes [30].

Hole number	Flow Rate l/day	Area m^2	Radius m	ga m^2/s	k_{app} m^2 ($\times 10^{-21}$)
IG202	0.014	5.20	0.0572	1.78×10^{-12}	1.94
IG201	0.025	5.91	0.0572	2.80×10^{-12}	3.24
NG252	0.250	0.26	0.0190	2.11×10^{-10}	445
A1X01	0.026	4.84	0.0508	3.16×10^{-12}	3.83
A1X02	0.010	5.74	0.0508	1.03×10^{-12}	1.07
A2X01	0.025	4.87	0.0508	3.02×10^{-12}	3.64
A2X02	0.015	5.13	0.0508	1.72×10^{-12}	1.92
A3X01	0.023	4.91	0.0508	2.75×10^{-12}	3.28
A3X02	0.001	4.93	0.0508	1.19×10^{-13}	0.08
BX01	0.055	4.87	0.0508	6.65×10^{-12}	8.81
DH36	0.250	4.38	0.0444	2.39×10^{-11}	46.4
DH38	0.055	4.04	0.0444	7.02×10^{-12}	9.62
DH40	0.005	4.34	0.0444	5.90×10^{-13}	0.59
DH42	0.030	4.35	0.0444	3.55×10^{-12}	4.51
DH42A	0.095	3.44	0.0444	1.42×10^{-11}	21.0
DH35	0.002	4.42	0.0444	2.37×10^{-13}	0.20
L1X00	0.028	3.72	0.0380	3.32×10^{-12}	4.33
DH215	0.004	1.22	0.0508	1.92×10^{-12}	2.19

Table 2. Observed flow rates for WIPP boreholes and apparent permeabilities based on eq. (19).

Hole number	Heat Flux (W/m^2)	Wall Temp. (°C)	Observed Peak Flux (m/s)	Calc. Scale, q_o (m/s) $k = 10^{-21}\ m^2$	$k = 10^{-20}\ m^2L$
A1041	63.3	35	3.0×10^{-11}	3.8×10^{-11}	8.7×10^{-11}
A1042	63.3	38	3.9×10^{-11}	3.9×10^{-11}	8.9×10^{-11}
B041	151.2	90	1.1×10^{-10}	1.3×10^{-10}	2.6×10^{-10}
B042	202.2	95	1.3×10^{-10}	1.7×10^{-10}	3.6×10^{-10}

Table 3. Flux calculations for heated boreholes.

Model	Equation	Cumulative Volume (m^3) $k = 10^{-21}\ m^2$	$k = 10^{-20}\ m^2$
Lateral semi-inf.	(37)	0.7	2.3
Lateral finite	(43)	0.4	0.4
Radial	(26)	6.7	40.6
Line sink	(31)	2.6	26.3

Table 4. Summary of results for cumulative volume at 200 years.

8. FIGURES

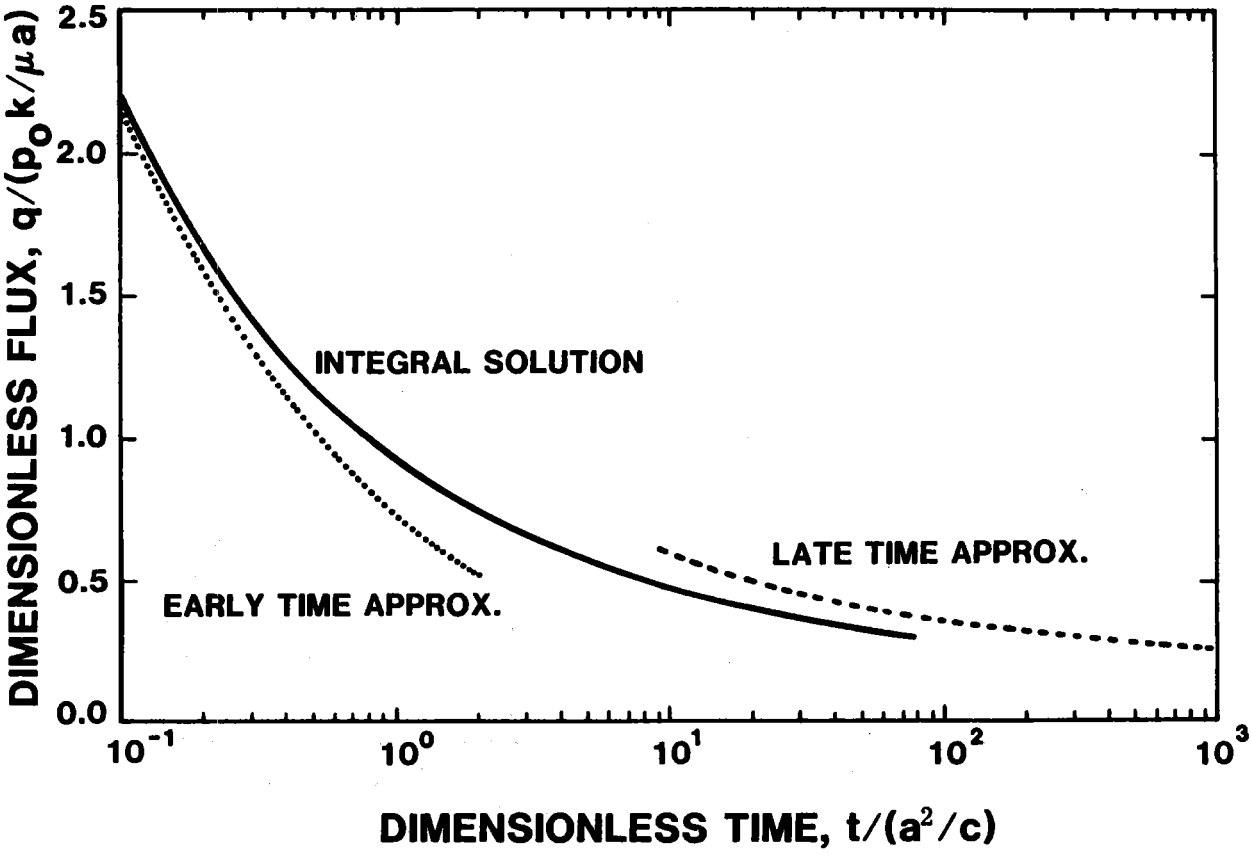

Figure 1. Flux to a circular tunnel or borehole.

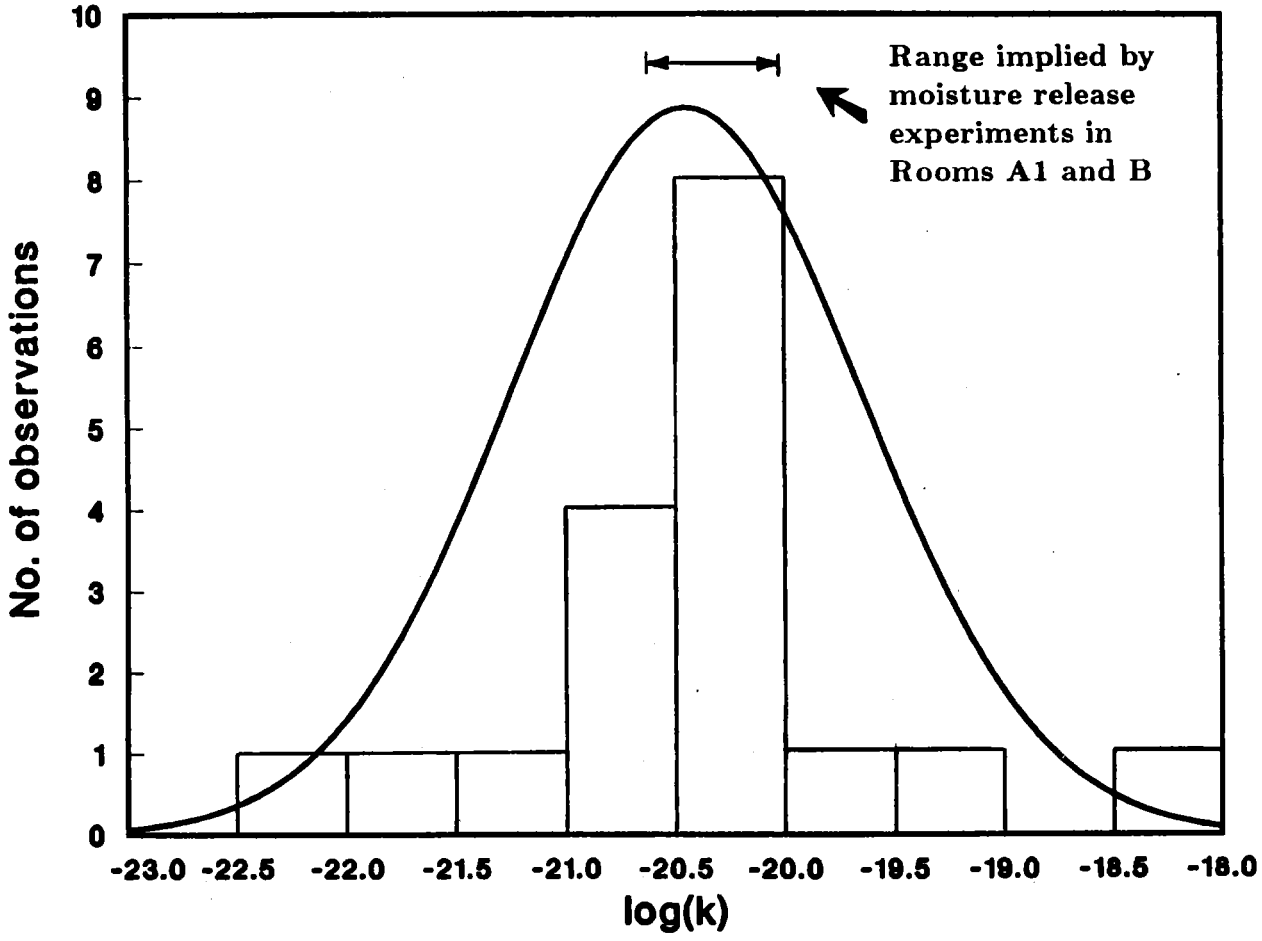

Figure 2. Apparent permeabilities based on BSEP data.

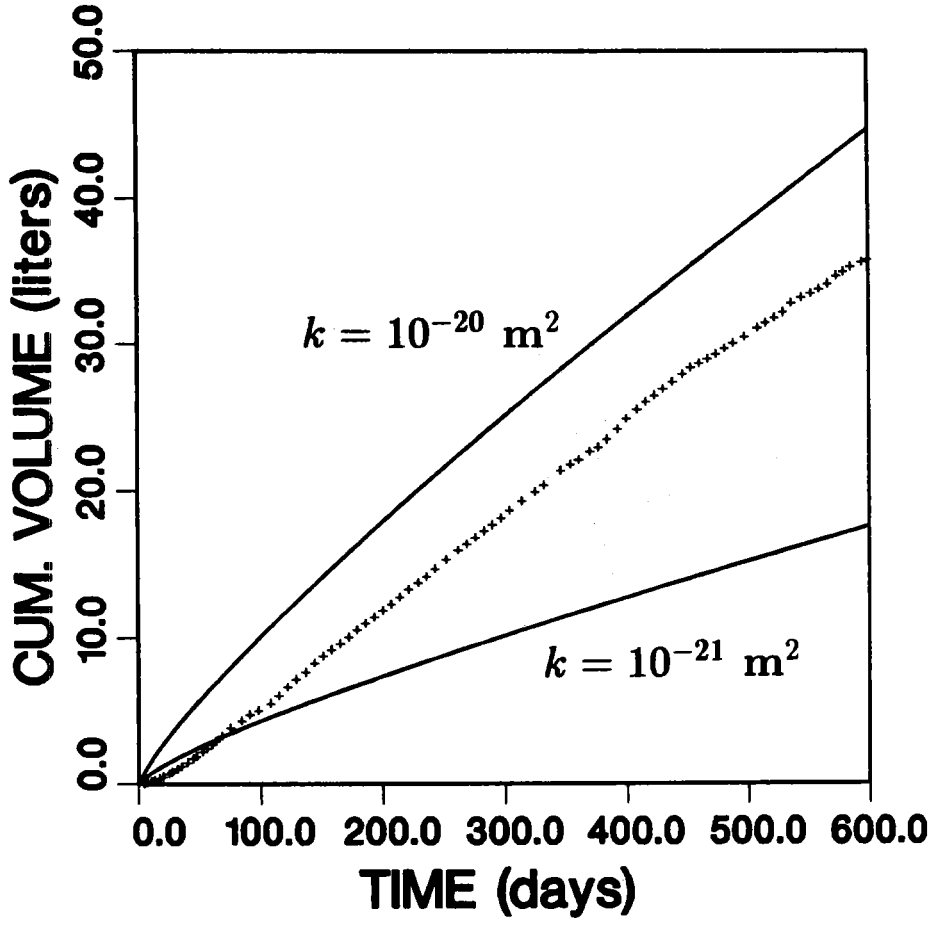

Figure 3. Comparison of observed (+) cumulative volume in borehole B042 with calculated brine inflow volume for k = $10^{-21}m^2$ and for k = $10^{-20}m^2$.

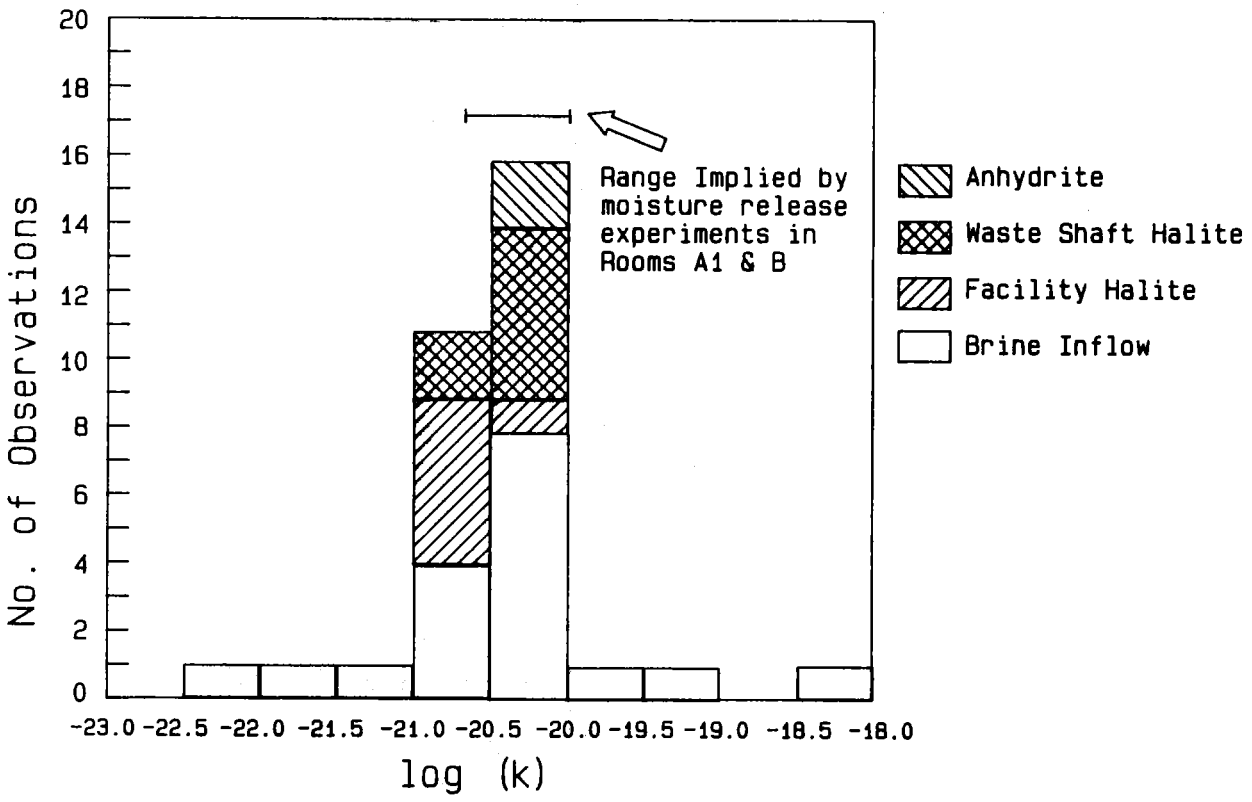

Figure 4. Brine permeabilities derived from in situ experiments.

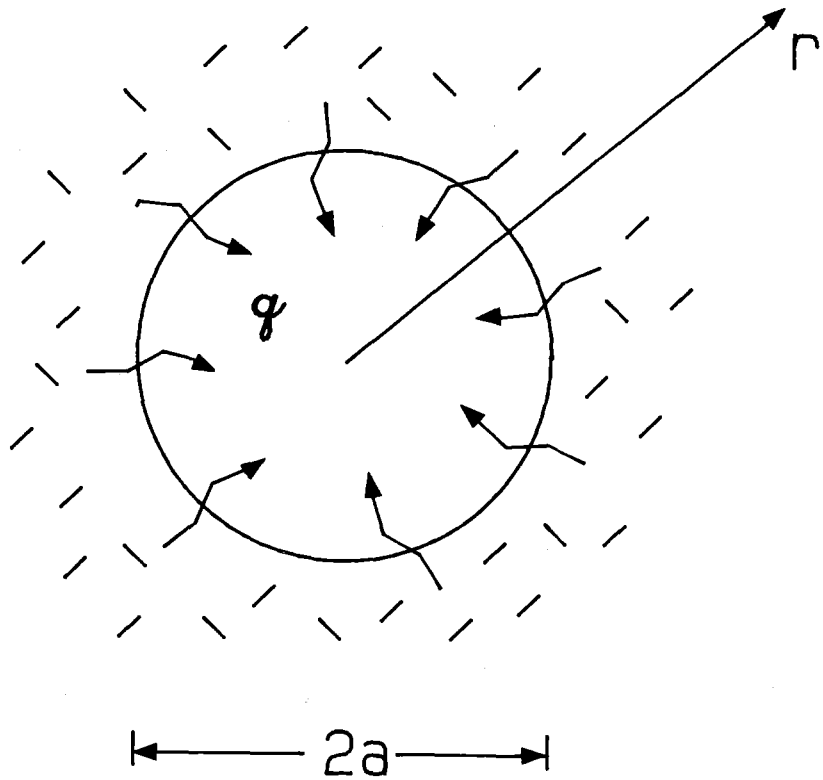

Figure 5. Geometry for radial flow to an isolated tunnel.

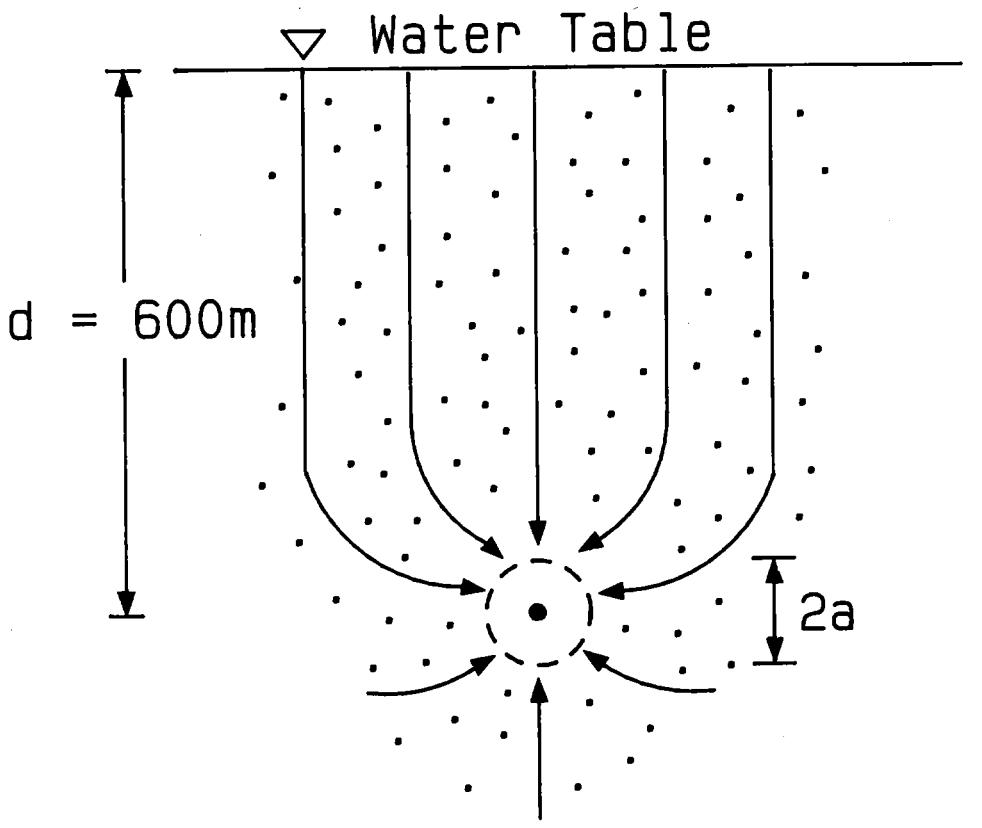

Figure 6. Geometry for steady flow to a line sink.

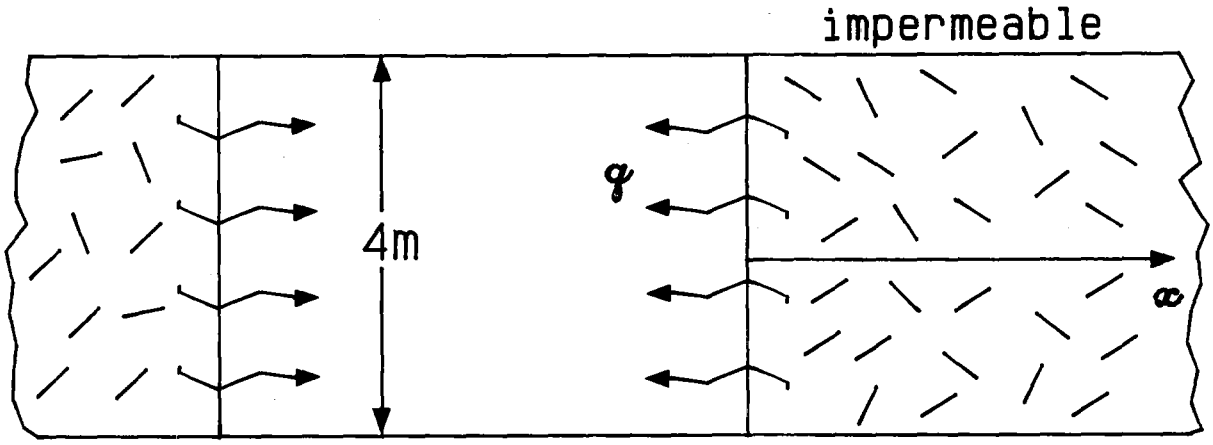

Figure 7. Geometry for lateral flow to an isolated room.

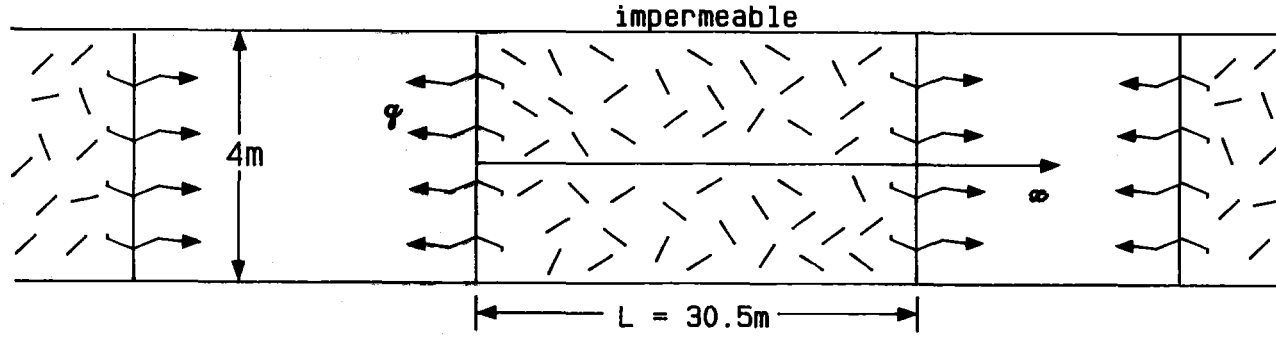

Figure 8. Geometry for lateral flow in an array of rooms.

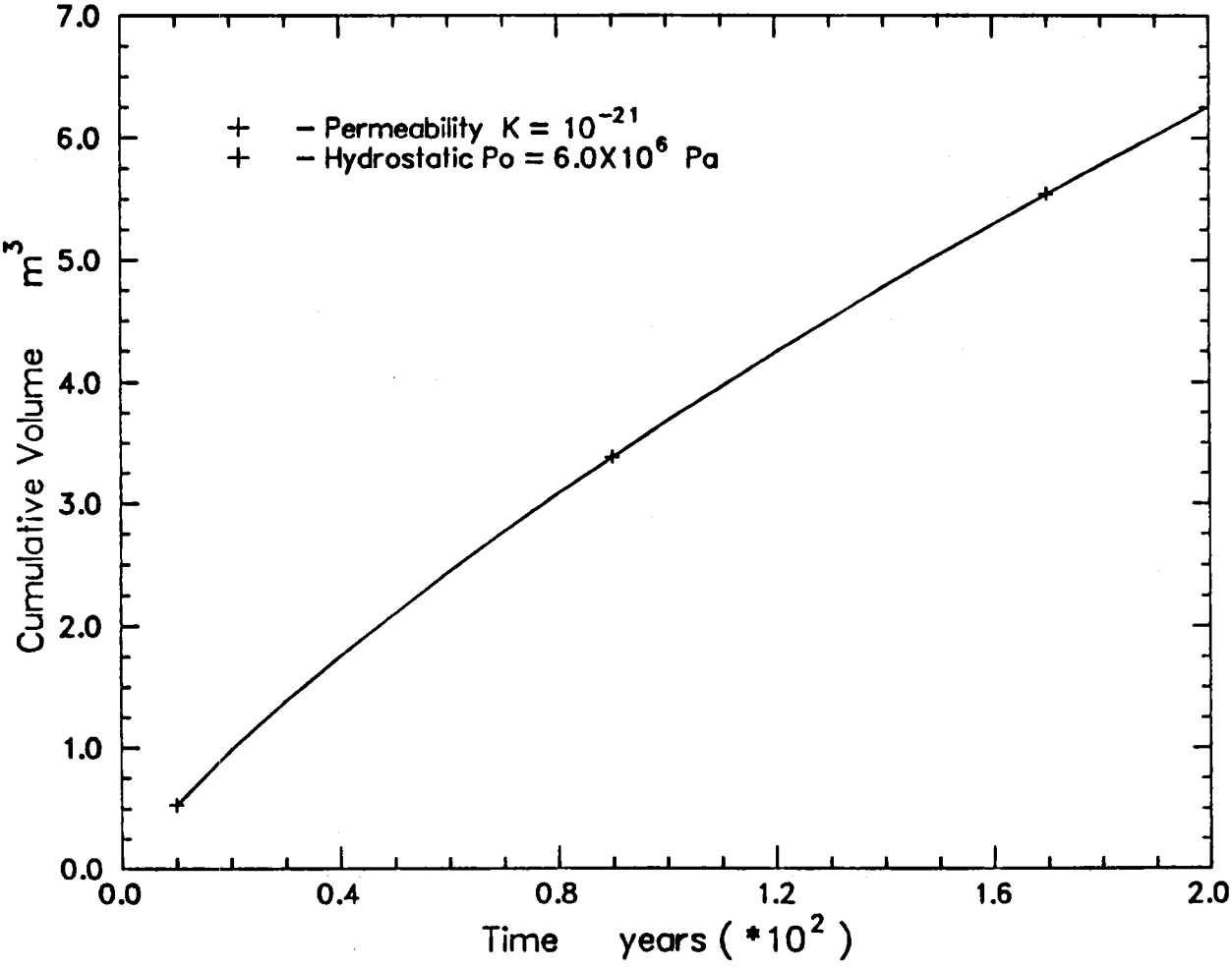

Figure 9. Calculated brine accumulation in a typical waste disposal room in a panel; Po = hydrostatic pressure; K = 1 nanodarcy.

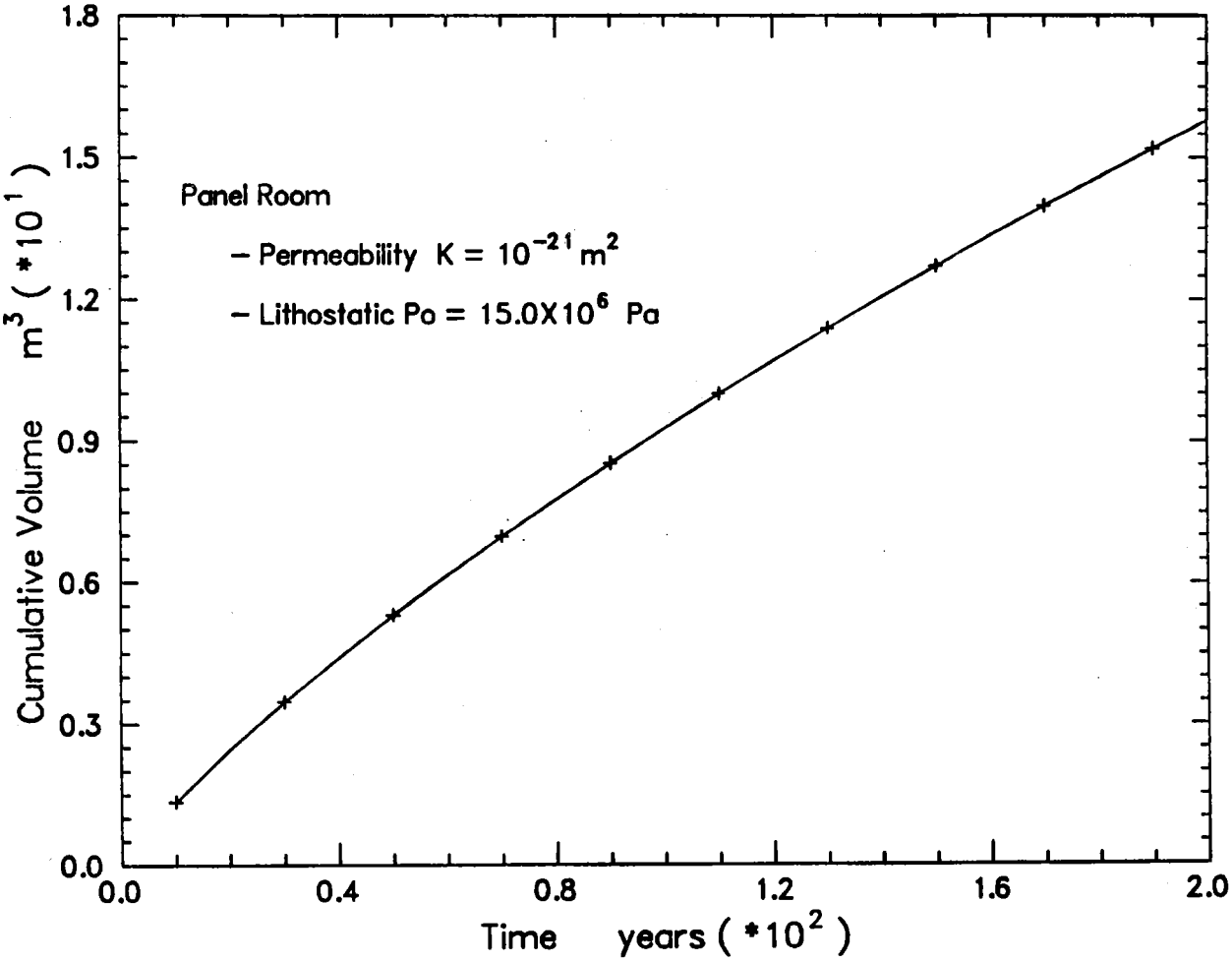

Figure 10. Calculated brine accumulation in a typical waste disposal room in a panel; Po = lithostatic pressure; K = 1 nanodarcy.

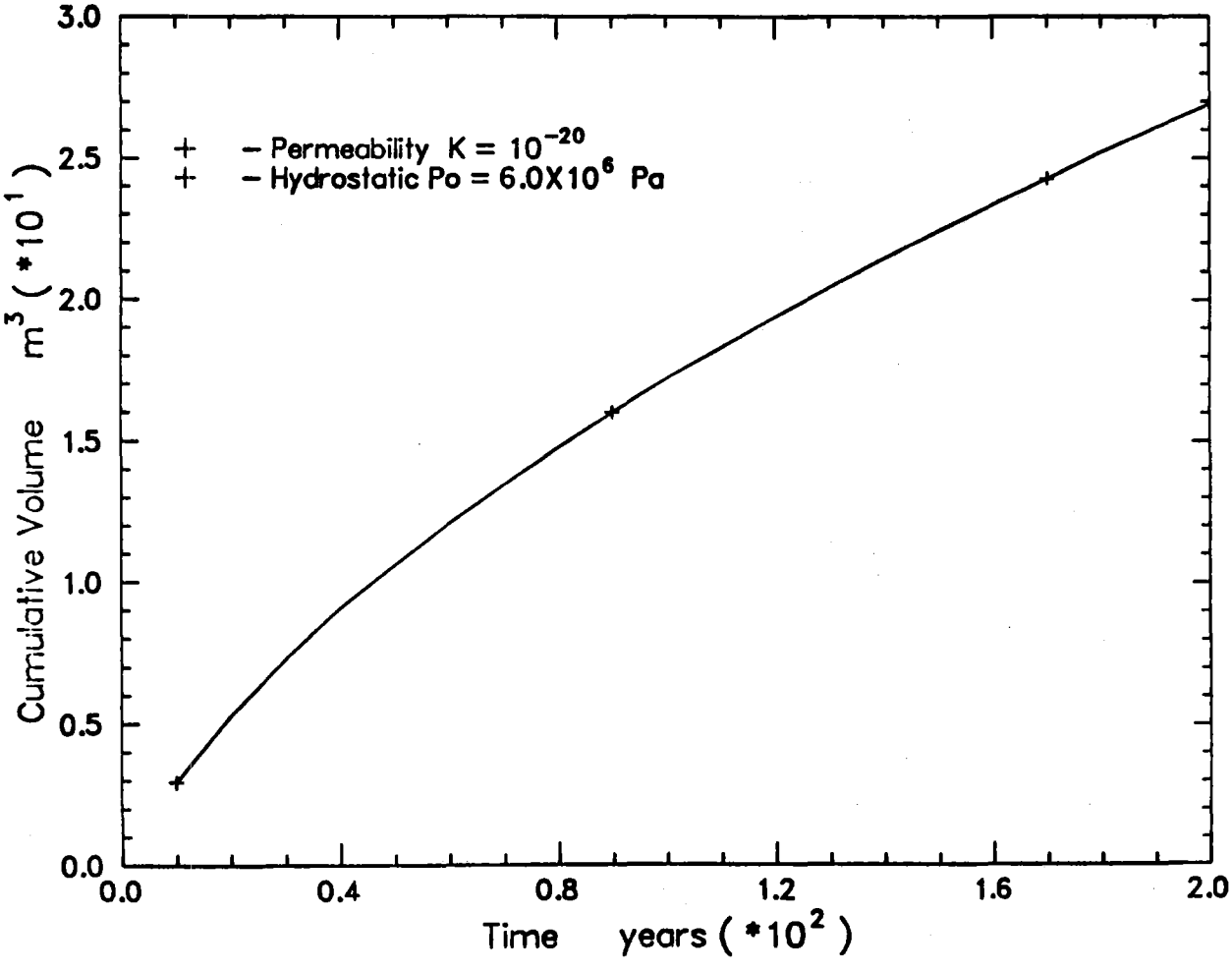

Figure 11. Calculated brine accumulation in a typical waste disposal room in a panel; Po = hydrostatic pressure; K = 10 nanodarcy.

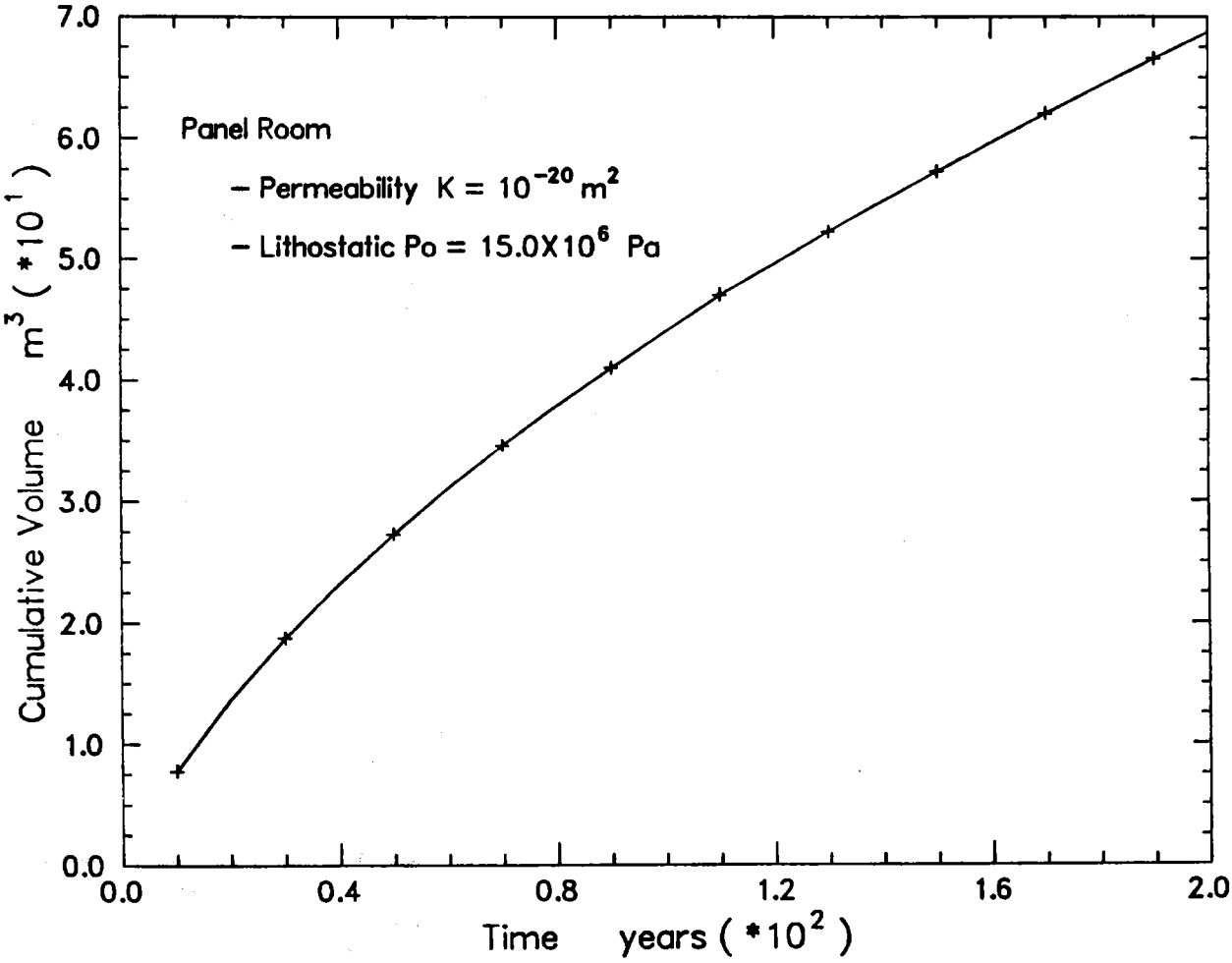

Figure 12. Calculated brine accumulation in a typical waste disposal room in a panel; Po = lithostatic pressure; K = 10 nanodarcy.

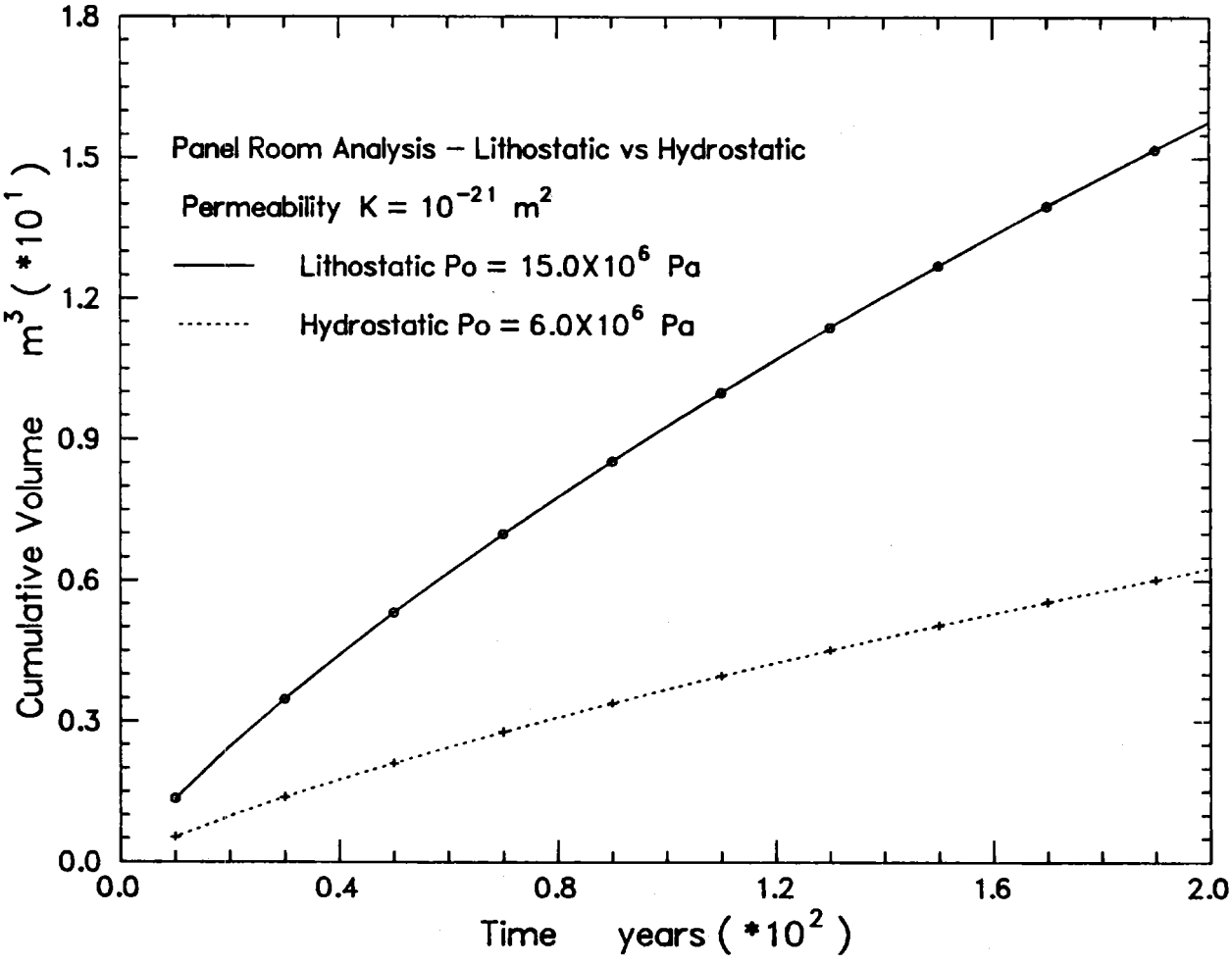

Figure 13. Sensitivity of calculated brine accumulation to initial pore pressure; typical room in a panel; K = 1 nanodarcy.

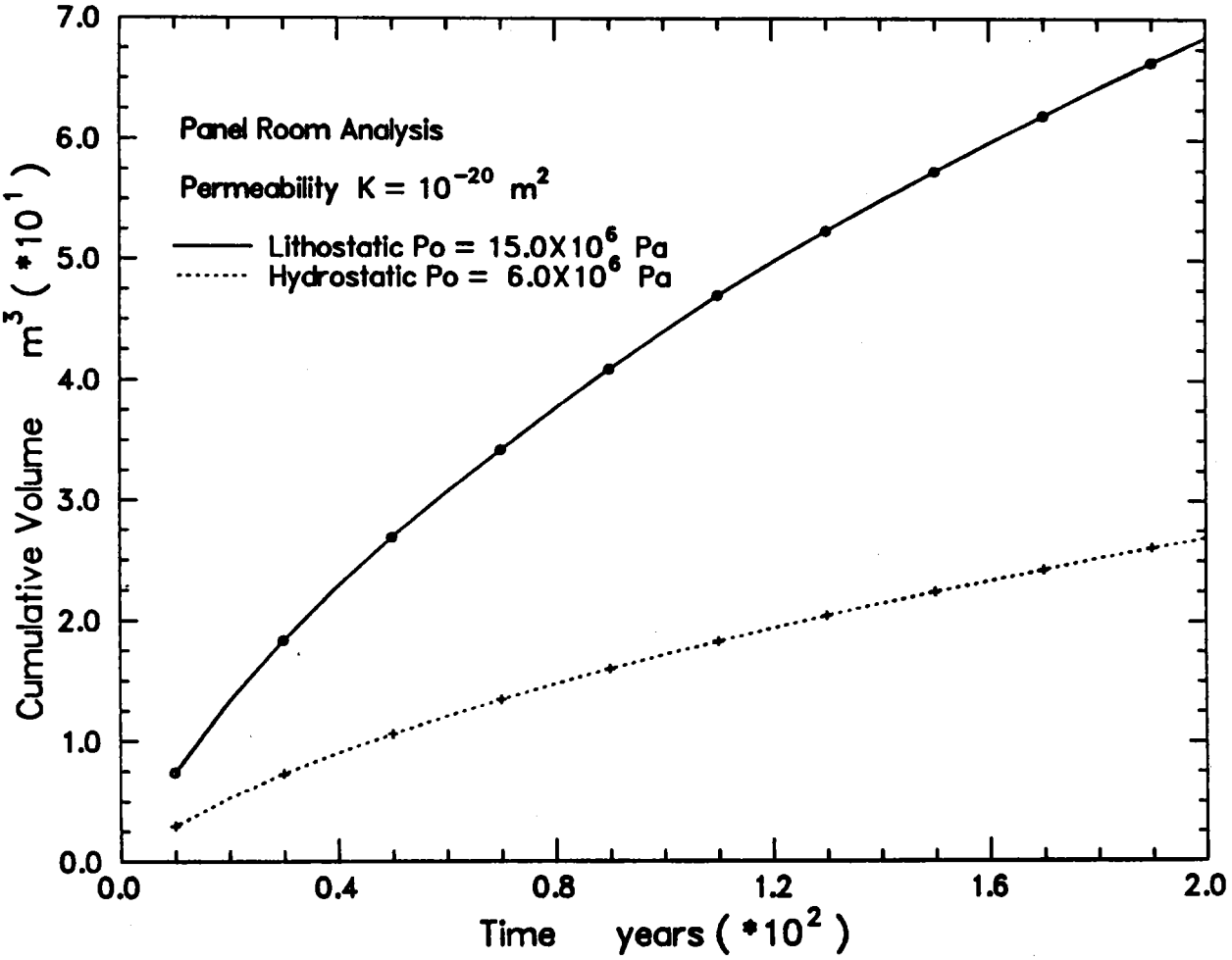

Figure 14. Sensitivity of calculated brine accumulation to initial pore pressure; typical room in a panel; K = 10 nanodarcy.

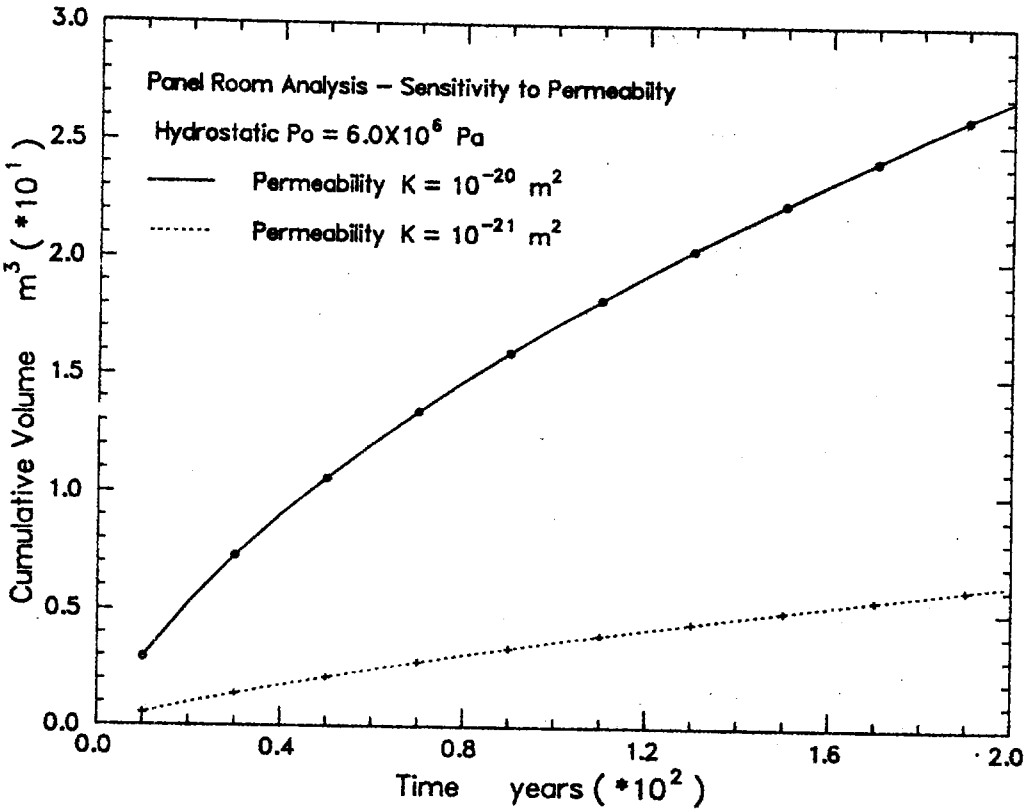

Figure 15. Sensitivity of calculated brine accumulation to host rock permeability; typical room in a panel; Po = hydrostatic pressure.

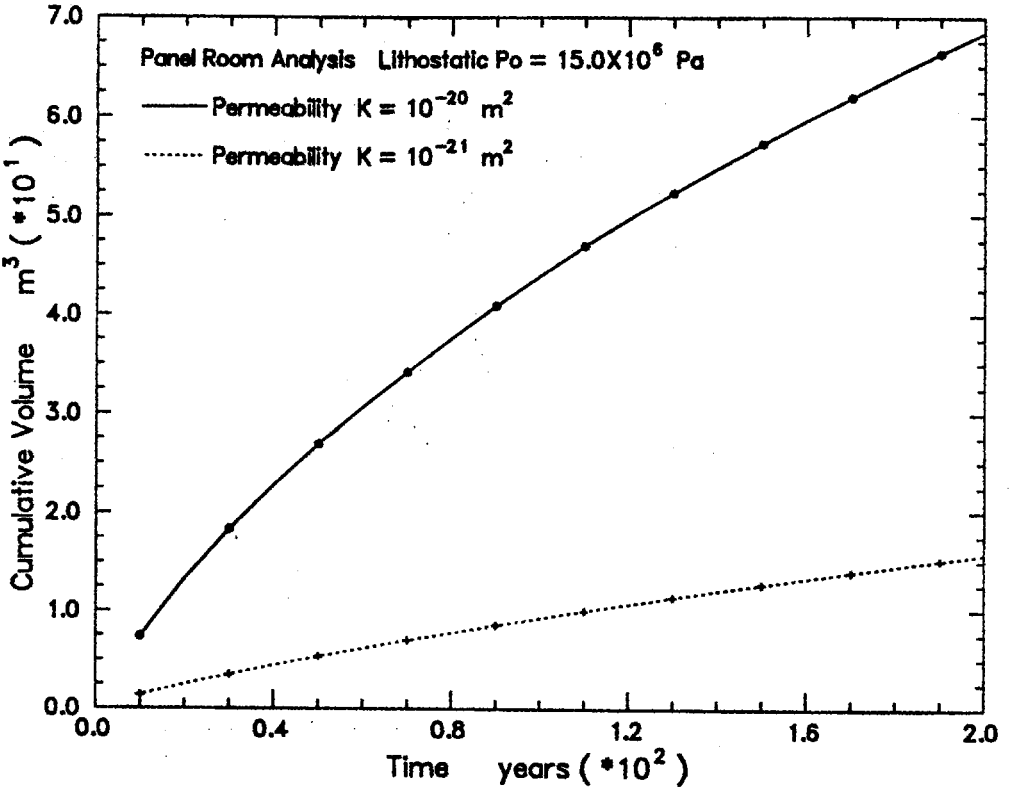

Figure 16. Sensitivity of calculated brine accumulation to host rock permeability; typical room in a panel; Po = lithostatic pressure.

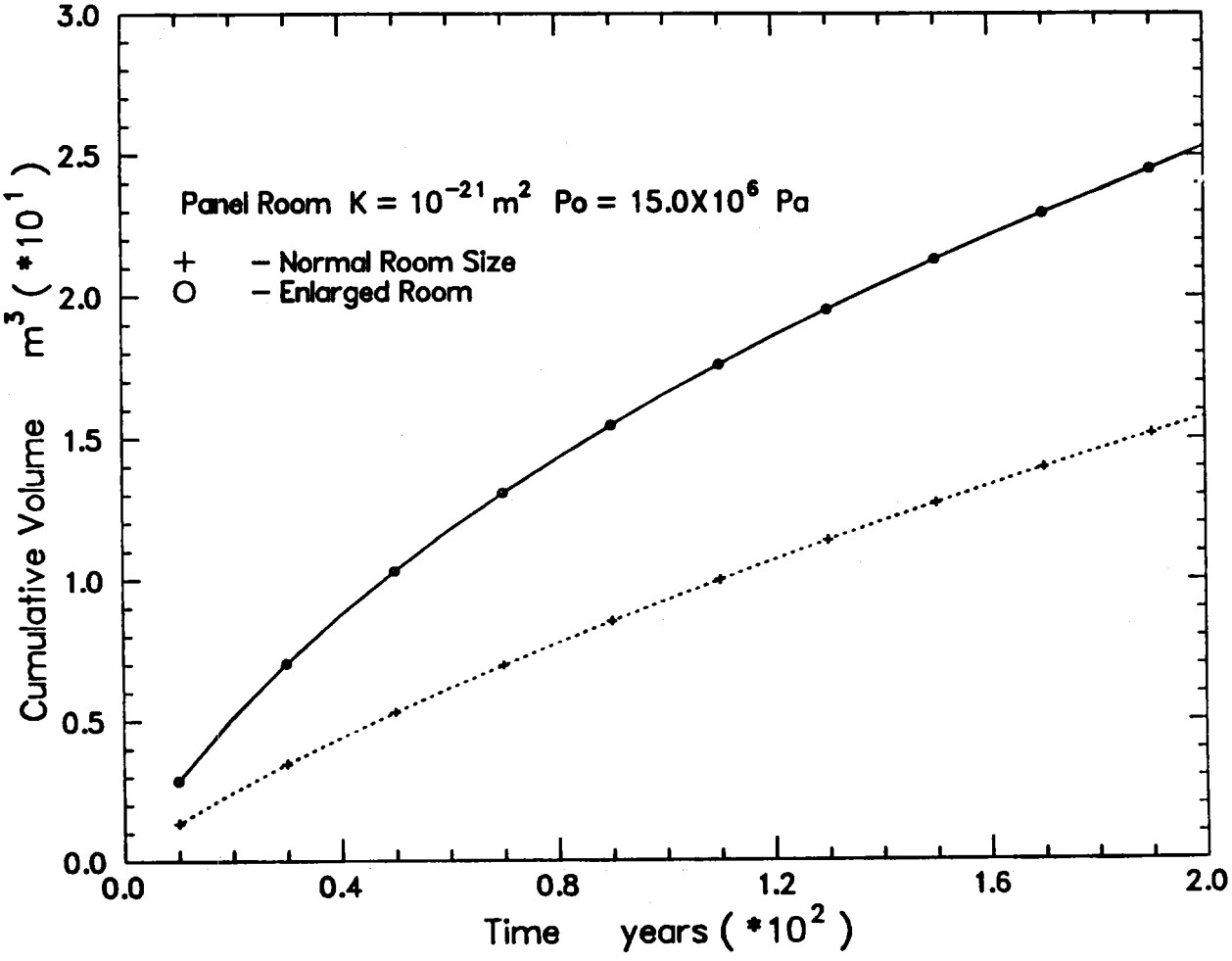

Figure 17. Effect of disturbed host rock zone on calculated brine accumulation; simulated with enlarged room; Po = lithostatic pressure; K = 1 nanodarcy.

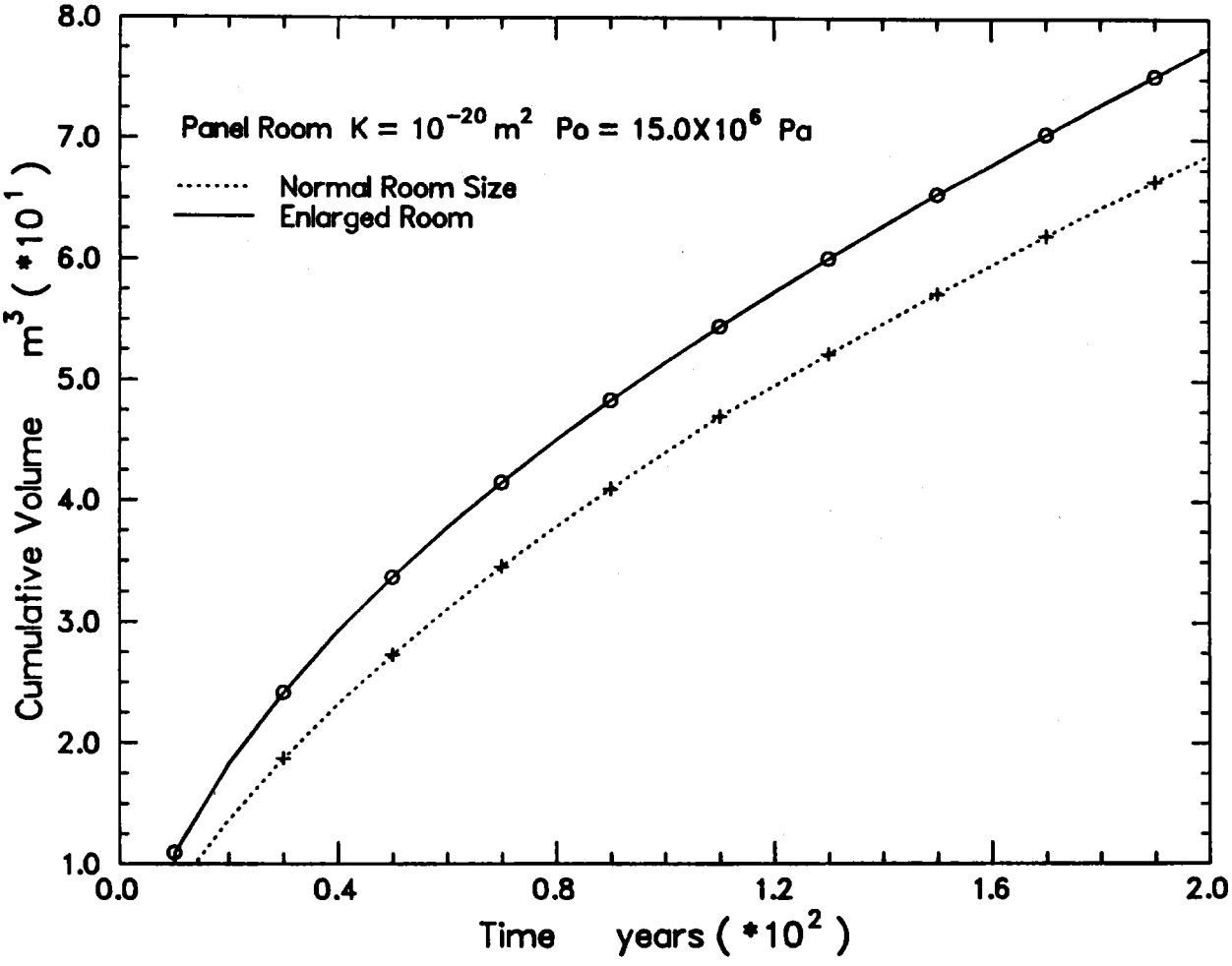

Figure 18. Effect of disturbed host rock zone on calculated brine accumulation; simulated with enlarged room; Po = lithostatic pressure; K = 10 nanodarcy.

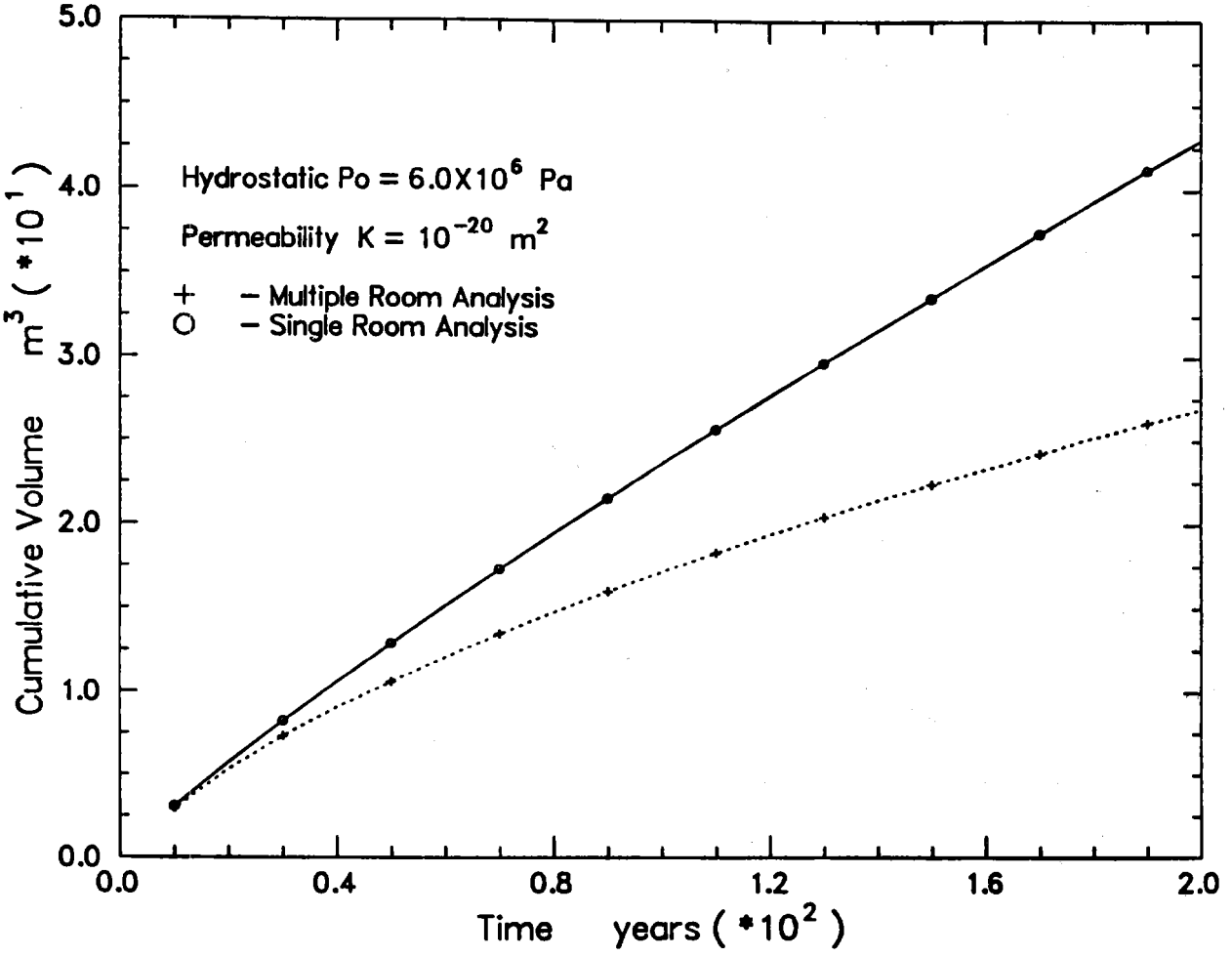

Figure 19. Effect of adjacent rooms in a panel on calculated brine accumulation; Po = hydrostatic pressure; K = 10 nanodarcy.

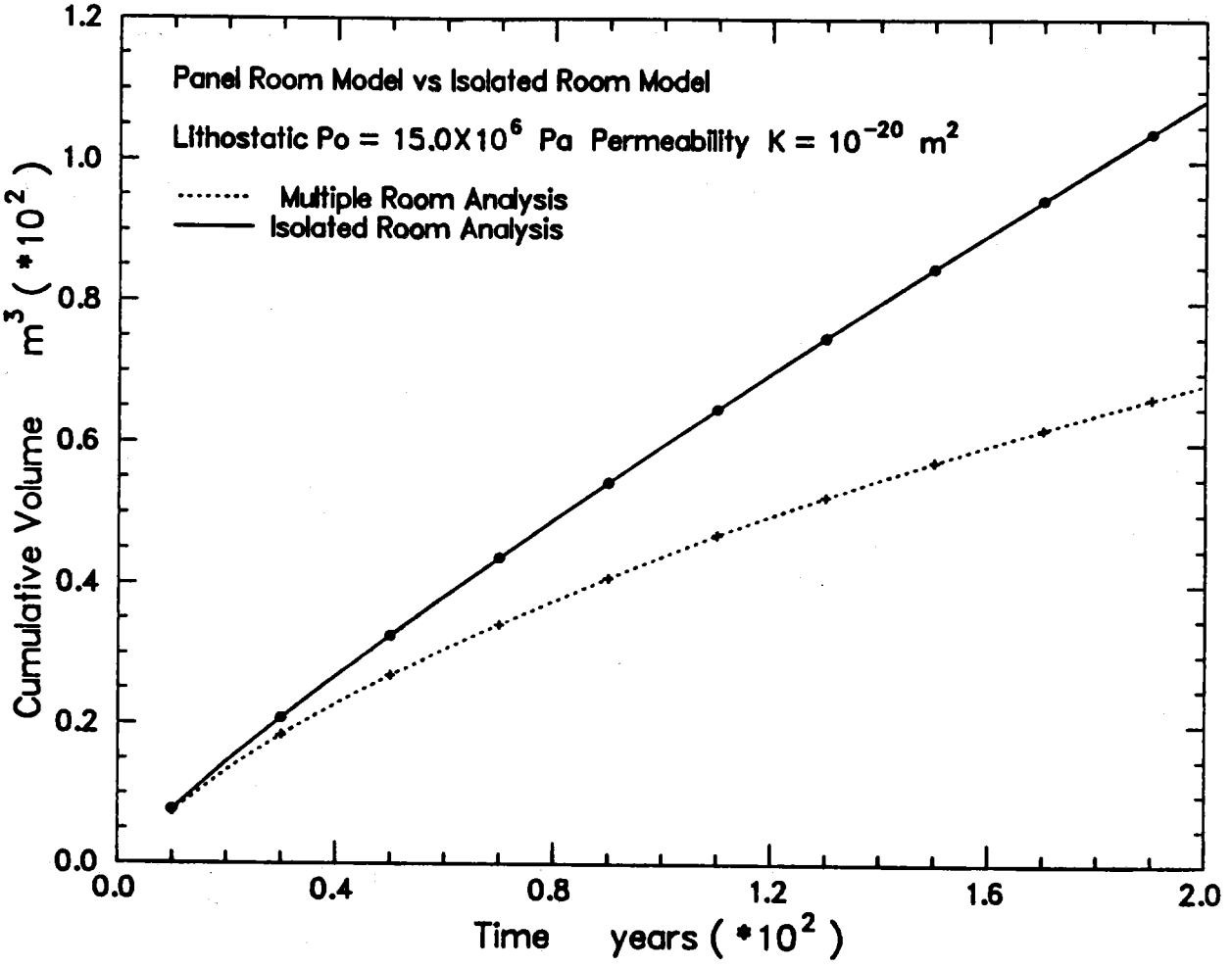

Figure 20. Effect of adjacent rooms in a panel on calculated brine accumulation; Po = lithostatic pressure; K = 10 nanodarcy.

10. APPENDIX A: MATERIAL PROPERTIES

The explicit relationships between the properties of salt and brine and the coefficients in the model equation (1) are as follows:

The fluid diffusivity, c, is given by

$$c = \frac{k}{\mu} \frac{2G(1 - \nu)}{1 - 2\nu} \left[\frac{B^2(1 + \nu_u)^2(1 - 2\nu)}{9(1 - \nu_u)(\nu_u - \nu)} \right] ,$$

$$\frac{1}{B} = 1 + \Phi_o \frac{K(1 - K_f/K_s)}{K_f(1 - K/K_s)} ,$$

$$\nu_u = \frac{3\nu + B(1 - 2\nu)(1 - K/K_s)}{3 - B(1 - 2\nu)(1 - K/K_s)} ,$$

where G is the elastic shear modulus, ν is Poisson's ratio under "drained" ($p = 0$) conditions, Φ_o is the reference porosity, K is the drained bulk modulus, K_f is the fluid bulk modulus, and K_S is the bulk modulus of the solid, mineral grains.

The source coefficient, b′, is given by

$$b' = \frac{4GB(1 + \nu_u)}{9(1 - \nu_u)} \left[\alpha_s + \frac{B(1 - \nu)(1 + \nu_u)}{2(\nu_u - \nu)} \Phi_o(\alpha_f - \alpha_s) \right] ,$$

where α_S and α_f are the thermal expansion coefficients for the solid and fluid constituents, respectively. Typical values of these properties for WIPP salt, used in the following calculations, are collected in the following table:

Property	Symbol	Value	Units
Thermal:			
Thermal conductivity	K	5.0	W m^{-1} K^{-1}
Thermal Diffusivity	κ	2.5×10^{-6}	m^2 s^{-1}
Elastic:			
Drained bulk modulus	K	20.7	GPa
Shear modulus	G	12.4	GPa
Drained Poisson ratio	ν	0.25	---
Fluid bulk modulus	K_f	2.0	GPa
Solid bulk modulus	K_s	23.5	GPa
Fluid expansivity (28°C)	α_f	4.6×10^{-4}	K^{-1}
Solid expansivity	α_s	1.2×10^{-4}	K^{-1}
Hydraulic:			
Permeability	k	10^{-21} to 10^{-20}	m^2
Porosity	Φ_o	0.001	---
Fluid viscosity (28°C)	μ	1.6×10^{-3}	Pa s
Derived:			
Fluid diffusivity	c	1.1×10^{-7} to 1.1×10^{-6}	m^2 s^{-1}
Source coefficient	b′	1.1×10^{6}	Pa K^{-1}
Pressure coefficient	B	0.926	---
Undrained Poisson ratio	ν_u	0.273	---
Diffusivity ratio	R^2	0.042 to 0.419	---

DISTRIBUTION

U. S. Department of Energy, (5)
Office of Civilian Radioactive Waste Management
Office of Geologic Repositories
Attn: Stephen H. Kale - RW-20
Associate Director
T. H. Isaacs - RW-20
Deputy Associate Director
James C. Bresee - RW-22
Director, Repository Coordination Div.
Ralph Stein - RW-23
Director, Engineering & Geotechnology
James P. Knight - RW-24
Director, Siting, Licensing and Quality Assurance
Forrestal Building
Washington, DC 20585

U. S. Department of Energy (3)
Albuquerque Operations Office
Attn: B. Twining
J. E. Bickel
R. Marquez, Director
Public Affairs Division
P.O. Box 5400
Albuquerque, NM 87185

U. S. Department of Energy (9)
WIPP Project Office (Carlsbad)
Attn: J. Tillman (4)
A. Hunt
T. Lukow (2)
V. Daub
B. Young
P.O. Box 3090
Carlsbad, NM 88221

U. S. Department of Energy
Research & Technical Support Division
Attn: D. E. Large
P. O. Box E
Oak Ridge, TN 37830

U. S. Department of Energy
Richland Operations Office
Nuclear Fuel Cycle & Production Division
Attn: R. E. Gerton
P.O. Box 500
Richland, WA 99352

U. S. Department of Energy (5)
Office of Defense Waste and Transportation Management
Attn: J. E. Dieckhoner - DP-122
L. H. Harmon ----- DP-121
A. Follett ------- DP-121
J. Mather -------- DP-121
M. Duff ---------- DP-121
Washington, DC 20545

U. S. Department of Energy (2)
Idaho Operations Office
Fuel Processing and Waste Management Division
785 DOE Place
Idaho Falls, ID 83402

U. S. Department of Energy (4)
Savannah River Operations Office
Defense Waste Processing Facility Project Office
Attn: S. Cowan
W. J. Brumley
P.O. Box A
Aiken, SC 29802

U.S. Nuclear Regulatory Commission (4)
Division of Waste Management
Attn: Michael Bell
Hubart Miller
Jacob Philip
NRC Library
Mail Stop 623SS
Washington, DC 20555

U. S. Nuclear Regulatory Commission
HLW Licensing Branch, Materials Section
Attn: F. R. Cook
MS 905 SS
Washington, DC 20555

U. S. Nuclear Regulatory Commission
CNWRA
Southwest Research Institute
Attn: John Latz
P.O. Box 28510
San Antonio, TX 78284

DISTRIBUTION

U. S. Geological Survey
Special Projects
Attn: R. Snyder
MS 913, Box 25046
Denver Federal Center
Denver, CO 80225

U. S. Geological Survey
Conservation Division
Attn: W. Melton
P.O. Box 1857
Roswell, NM 88201

U. S. Geological Survey
Water Resources Division
Attn: H. Lee Case
Suite 200
4501 Indian School, NE
Albuquerque, NM 87110

State of New Mexico (3)
Environmental Evaluation Group
Attn: Robert H. Neill, Director
P.O. Box 3149
Carlsbad, NM 87221

New Mexico Department of
Energy and Minerals
Attn: Kasey LaPlante, Librarian
P.O. Box 2770
Santa Fe, NM 87501

New Mexico Bureau of Mines
and Mineral Resources (2)
Attn: F. E. Kottolowski, Director
J. Hawley
Socorro, NM 87801

Battelle Pacific Northwest
Laboratories
Attn: D. J. Bradley
Battelle Boulevard
Richland, WA 99352

Bechtel Inc. (5)
45-11-B34
Attn: E. Weber
M. Beathard
H. Taylor
P. Frobenius
D. L. Wu
P.O. Box 3965
San Francisco, CA 94119

INTERA Technologies, Inc. (2)
Attn: G. E. Grisak
J. F. Pickens
6850 Austin Center Blvd., #300
Austin, TX 78731

INTERA Technologies, Inc.
Attn: Wayne Stensrud
P.O. Box 2123
Carlsbad, NM 88221

IT Corporation
Attn: R. McKinney
P.O. Box 2078
Carlsbad, NM 88221

IT Corporation (3)
Attn: M. Smith
W. R. Coons
J. Myers
2340 Alamo, SE, Suite 306
Albuquerque, NM 87106

RE/SPEC, Inc. (7)
Attn: P. F. Gnirk
L. L. Van Sambeek
D. B. Blankenship
T. Brandshang
G. Callahan
T. Pfeifle
J. L. Ratigan
P. O. Box 725
Rapid City, SD 57709

RE/SPEC, Inc.
Attn: S. W. Key
P.O. Box 14984
Albuquerque NM 87191

E. I. Dupont de Nemours Company (6)
Savannah River Laboratory
Attn: N. Bibler
E. L. Albenisius
M. J. Plodinec
G. G. Wicks
C. Jantzen
J. A. Stone
Aiken, SC 29801

Dupont Company
Building 704-S
Attn: Richard G. Baxter
Savannah River Plant
Aiken, SC 29808

DISTRIBUTION

SAIC
Attn: George Dymmel
101 Convention Center Dr.
Las Vegas, NV 89109

Systems, Science, and Software (2)
Attn: E. Peterson
P. Lagus
Box 1620
La Jolla, CA 92038

Dr. Edwin Roedder
Department of Earth Planetary Sciences
Harvard University
Cambridge, MA 02138

University of Arizona
Attn: J. G. McCray
Department of Nuclear Engineering
Tucson, AZ 85721

University of Arizona
Attn: J. J. K. Daemen
Department of Mining and
Geological Engineering
Tucson, AZ 85721

University of New Mexico (2)
Attn: D. G. Brookins
Library
Geology Department
Albuquerque, NM 87131

The Pennsylvania State University
Materials Research Laboratory
Attn: Della Roy
University Park, PA 16802

Westinghouse Electric Corporation (9)
Attn: Library
W. Moffitt
V. DeJong
W. Chiquelin
T. Dillon
V. Likar
J. Johnson
J. Sadler
R. Kehrman
P.O. Box 2078
Carlsbad, NM 88221

National Academy of Sciences, WIPP Panel:

Dr. Konrad B. Krauskopf
Department of Geology
Panama Street
Stanford University
Stanford, CA 94305

Dr. Frank L. Parker
Department of Environmental and
Water Resources Engineering
Vanderbilt University
Nashville, TN 37235

Dr. John O. Blomeke
Route 3
Sandy Shore Road
Lenoir City, TN 37771

Dr. John D. Bredehoeft
Western Region Hydrologist
Water Resources Division
U.S. Geological Survey
345 Middlefield Road
Menlo Park, CA 94025

Dr. Karl P. Cohen
928 N. California Avenue
Palo Alto, CA 94303

Dr. Fred M. Ernsberger
250 Old Mill Road
Pittsburgh, PA 15238

Dr. Rodney C. Ewing
Department of Geology
University of New Mexico
200 Yale, NE
Albuquerque, NM 87131

Dr. Charles Fairhurst
Department of Civil and
Mineral Engineering
University of Minnesota
500 Pillsbury Dr. SE
Minneapolis, MN 55455

Dr. William R. Muehlberger
Department of Geological Sciences
University of Texas at Austin
P.O. Box 7909
Austin, TX 78712

DISTRIBUTION

Dr. D'Arcy A. Shock
233 Virginia
Ponca City, OK 74601

Dr. Peter B. Myers,
Staff Director
National Academy of Sciences
Committee on Radioactive
Waste Management
2101 Constitution Avenue
Washington, DC 20418

Ms. Remi Langum
Staff Officer
Board on Radioactive Waste
Management
2101 Constitution Avenue
Washington, D. C. 20418

Hobbs Public Library
Attn: Ms. Marcia Lewis, Librarian
509 N. Ship Street
Hobbs, NM 88248

New Mexico Tech
Martin Speere Memorial Library
Campus Street
Socorro, NM 87810

New Mexico State Library
Attn: Ms. Ingrid Vollenhofer
P.O. Box 1629
Santa Fe, NM 87503

Zimmerman Library
Attn: Zanier Vivian
University of New Mexico
Albuquerque, NM 87131

U. S. Department of Energy
ATTN: National Atomic Museum Library
Albuquerque Operations Office
P.O. Box 5400
Albuquerque, NM 87113

WIPP Public Reading Room
Carlsbad Municipal Library
Attn: Lee Hubbard, Head Librarian
101 S. Halagueno St.
Carlsbad, NM 88220

Thomas Brannigan Library
Attn: Don Dresp, Head Librarian
106 W. Hadley St.
Las Cruces, NM 88001

Roswell Public Library
Attn: Ms. Nancy Langston
301 N. Pennsylvania Avenue
Roswell, NM 88201

Pannell Library
Attn: Ms. Ruth Hill
New Mexico Junior College
Lovington Highway
Hobbs, NM 88240

Argonne National Laboratory (3)
Attn: D. Hambeley
W. Harrison
M. Steindler
9700 South Cass Avenue
Argonne, IL 60439

Los Alamos Scientific Laboratory
Attn: B. Erdal, CNC-11
Los Alamos, NM 87545

Oak Ridge National Laboratory (4)
Attn: R. E. Blanko
E. Bondietti
C. Claiborne
G. H. Jenks
Box Y
Oak Ridge, TN 37830

Oak Ridge National Laboratory
Bldg. 2001
Ecological Sciences Information Center
Attn: C. S. Fore
P.O. Box X
Oak Ridge, TN 37830

Rockwell International (2)
Attn: W. S. Bennett
C. E. Wickland
Rocky Flats Plant
Golden, CO 80401

Rockwell International (3)
Atomics International Division
Rockwell Hanford Operations
Attn: J. Nelson (HWVP)
P. Salter
W. W. Schultz
P.O. Box 800
Richland, WA 99352

DISTRIBUTION

Svensk Karnbransleforsorjning AB
Attn: Fred Karlsson
Project KBS
Karnbranslesakerhet
Box 5864
10248 Stockholm
SWEDEN

Institut fur Tieflagerung (5)
Attn: K. Kuhn
N. Jockwer
P. Faber
G. Stampendahl
W. Hansel
Theodor-Heuss-Strasse 4
D-3300 Braunschweig
FEDERAL REPUPLIC OF GERMANY

Wolfgang R. Fischle
c/o Deutsche Gesellschaft zum
Bau und Betrieb von Endlagern
fur Abfallstoffe mbH (DBE)
Woltorfer Strabe 74
D-3150 Peine 1
FEDERAL REPUBLIC OF GERMANY

Bundesanstalt fur Geowissenschaften
und Rohstoffe
Attn: Michael Langer
Postfach 510 153
3000 Hannover 51
FEDERAL REPUBLIC OF GERMANY

Hahn-Mietner-Institut fur
Kernforschung (2)
Attn: Werner Lutze
Klaus Eckart Maass
Glienicker Strasse 100
100 Berlin 39
FEDERAL REPUBLIC OF GERMANY

Bundesministerium fur Forschung und
Technologie
Attn: Rolf-Peter Randl
Postfach 200 706
5300 Bonn 2
FEDERAL REPUBLIC OF GERMANY

Physikalisch-Technische Bundesanstalt
Attn: Peter Brenneke
Postfach 33 45
D-3300 Braunschweig
FEDERAL REPUBLIC OF GERMANY

Kernforschug Karlsruhe (3)
Attn: R. Koster
Reinhard Kraemer
K. D. Closs
Postfach 3640
7500 Karlsruhe
FEDERAL REPUBLIC OF GERMANY

Atomic Energy of Canada, Ltd. (2)
Attn: Peter Haywood
John Tait
Whiteshell Research Estab.
Pinewa, Manitoba, ROE 1LO
CANADA

Dr. D. K. Mukerjee
Ontario Hydro Research Lab
800 Kipling Avenue
Toronto, Ontario, MBZ 554
CANADA

Studiecentrum Voor Kernenergie (2)
Attn: Mr. A. Bonne
Pierre Van Iseghem
Centre D'Energie Nucleaire
SCK/CEN
Boeretang 200
B-2400 Mol
BELGIUM

Claude Sombret
Centre D'Etudes Nucleaires
De La Vallee Rhone
CEN/VALRHO
S.D.H.A. BP 171
30205 Bagnols-Sur-Ceze
FRANCE

Mr. Jean-Pierre Olivier
OECD Nuclear Energy Agency
Division of Radiation Protection
and Waste Management
38, Boulevard Suchet
75016 Paris
FRANCE

D. R. Knowles
British Nuclear Fuels, plc
Risley, Warrington, Cheshire WA3 6AS
1002607
GREAT BRITAIN

DISTRIBUTION

Shingo Tashiro
Japan Atomic Energy Research Institute
Tokai-Mura, Ibaraki-Ken
319-11
JAPAN

Netherlands Energy Research Foundation
ECN (2)
Attn: Tuen Deboer, Mgr.
L. H. Vons
3 Westerduinweg
P.O. Box 1
1755 ZG Petten
NETHERLANDS

Sandia Internal:

1510 J. W. Nunziato
1511 D. F. McTigue (10)
1520 C. W. Peterson
1521 R. D. Krieg
1521 H. S. Morgan
1820 R. E. Whan
1821 S. H. Weissman
1830 M. J. Davis
1831 J. W. Munford
1831 N. R. Sorensen
1832 W. B. Jones
1832 J. A. Van Den Avyle
1833 G. A. Knorovsky
1840 R. J. Eagan
3141 S. A. Landenberger (5)
3151 W. L. Garner, For: DOE/TIC (Unlimited Release) (3)
3154-1 C. H. Dalin, For: DOE/OSTI (8)
6000 D. L. Hartley
6230 W. C. Luth
6232 W. R. Wawersik
6233 T. M. Gerlach
6233 J. L. Krumhansl
6233 H. W. Stockman
6300 R. W. Lynch
6310 T. O. Hunter
6313 T. Blejwas
6330 W. D. Weart
6330 G. R. Romero
6331 A. R. Lappin
6331 R. L. Beauheim
6331 D. J. Borns
6331 P. B. Davies
6331 S. J. Lambert
6331 R. Z. Lawson
6331 K. L. Robinson
6332 L. D. Tyler
6332 R. Beraun (10)
6332 B. M. Butcher
6332 R. V. Matalucci
6332 M. A. Molecke
6332 D. E. Munson
6332 E. J. Nowak (50)
6332 R. J. Roginski
6332 J. C. Stormont
6332 T. M. Torres
6332 Sandia WIPP Central Files 590PS/BT (2)
6333 T. M. Schultheis
6334 D. R. Anderson
6334 S. G. Bertram-Howery
6334 K. Brinster
6334 L. H. Brush
6334 M. S. Y. Chu
6334 L. S. Gomez
6334 R. Hunter
6334 M. G. Marietta
6334 R. P. Rechard
6334 A. K. Rutledge
7100 C. D. Broyles
7110 J. D. Plimpton
7116 S. R. Dolce
7116 C. W. Cook
7120 M. J. Navratil
7125 R. L. Rutter
7125 J. T. McIlmoyle
7125 J. J. Loukota
7130 J. O. Kennedy
7133 R. D. Statler
7133 J. W. Mercer
7133 H. C. Walling
7135 P. D. Seward
8310 R. W. Rhode
8314 S. L. Robinson
8314 N. R. Moody
8314 M. W. Perra
8315 L. A. West
8524 P. W. Dean (SNLL Library)